iScience

CellPress
OPEN ACCESS

Article

Beat-to-beat dynamic regulation of intracellular pH in cardiomyocytes

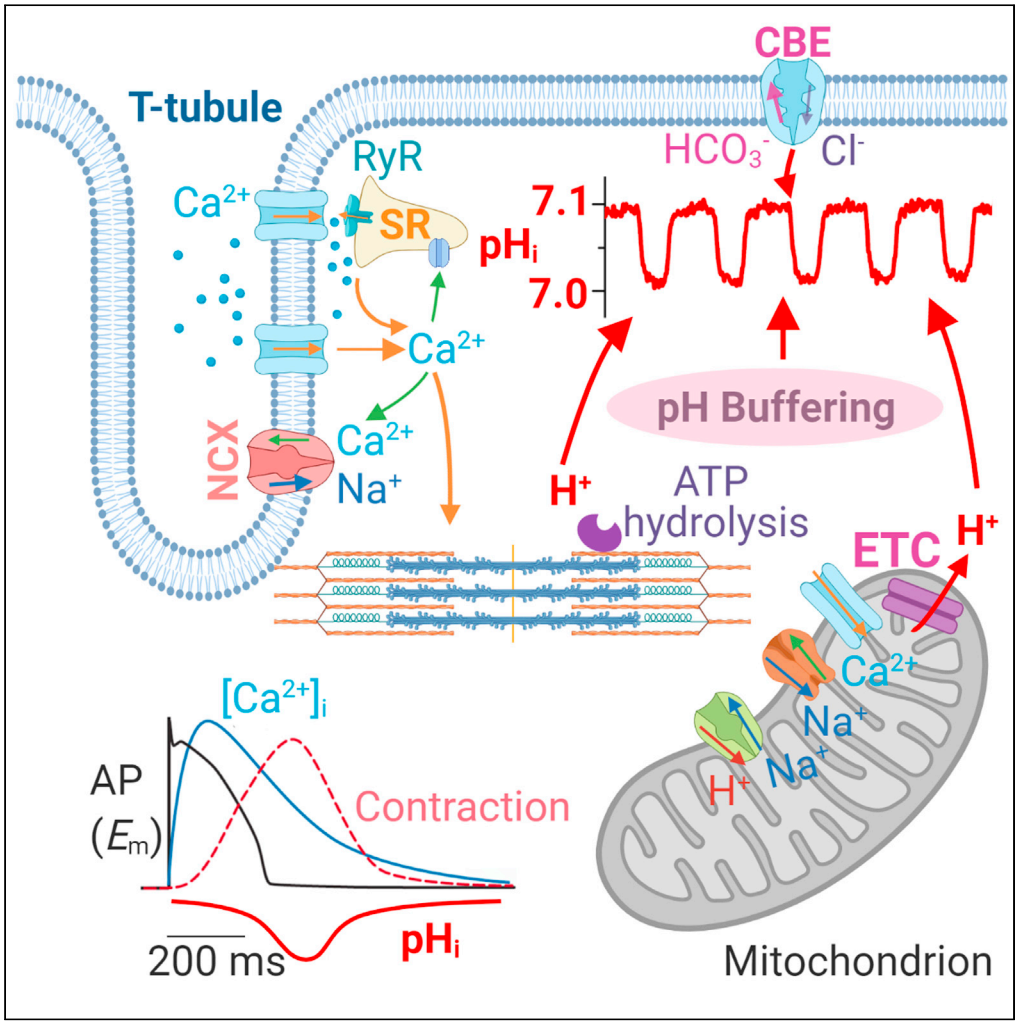

Yankun Lyu, Phung N. Thai, Lu Ren, ..., Ye Chen-Izu, Nipavan Chiamvimonvat, Xiao-Dong Zhang

xdzhang@ucdavis.edu

Highlights

Cardiomyocytes exhibit beat-to-beat cellular acidification, termed "pH_i transient."

pH_i transients are coupled to cardiomyocyte contractions and are tightly regulated

Inhibitions of the mitochondrial electron transport chain attenuate pH_i transients

pH_i transients may reflect a rhythmic metabolic status in cardiomyocytes

Lyu et al., iScience 25, 103624
January 21, 2022
https://doi.org/10.1016/j.isci.2021.103624

iScience

CellPress
OPEN ACCESS

Article

Beat-to-beat dynamic regulation of intracellular pH in cardiomyocytes

Yankun Lyu,[1] Phung N. Thai,[1] Lu Ren,[1] Valeriy Timofeyev,[1] Zhong Jian,[2] Seojin Park,[3] Kenneth S. Ginsburg,[2] James Overton,[1] Julie Bossuyt,[2] Donald M. Bers,[2] Ebenezer N. Yamoah,[3] Ye Chen-Izu,[1,2,4] Nipavan Chiamvimonvat,[1,2,5] and Xiao-Dong Zhang[1,5,6,*]

SUMMARY

The mammalian heart beats incessantly with rhythmic mechanical activities generating acids that need to be buffered to maintain a stable intracellular pH (pH_i) for normal cardiac function. Even though spatial pH_i non-uniformity in cardiomyocytes has been documented, it remains unknown how pH_i is regulated to match the dynamic cardiac contractions. Here, we demonstrated beat-to-beat intracellular acidification, termed pH_i transients, in synchrony with cardiomyocyte contractions. The pH_i transients are regulated by pacing rate, Cl^-/HCO_3^- transporters, pH_i buffering capacity, and β-adrenergic signaling. Mitochondrial electron-transport chain inhibition attenuates the pH_i transients, implicating mitochondrial activity in sculpting the pH_i regulation. The pH_i transients provide dynamic alterations of H^+ transport required for ATP synthesis, and a decrease in pH_i may serve as a negative feedback to cardiac contractions. Current findings dovetail with the prevailing three known dynamic systems, namely electrical, Ca^{2+}, and mechanical systems, and may reveal broader features of pH_i handling in excitable cells.

INTRODUCTION

The heart has the most extraordinary metabolic demands per gram of tissue among excitable cells because of the constant mechanical work (Doenst et al., 2013; Wang et al., 2010). ATP powers cardiac contraction. The production of ATP generates H^+ and CO_2 in aerobic reactions and lactic acid in anaerobic metabolism, yielding acidic products that alter intracellular pH (pH_i). pH_i is a crucial regulator of cellular structure and function(Casey et al., 2010; Cordat and Casey, 2009). Cells employ mobile HCO_3^-, less mobile protein buffers and H^+-equivalent transporters to maintain a stable pH_i (Casey et al., 2010; Roos and Boron, 1981). In the absence of H^+ regulatory mechanisms, large pH_i swings ensue(Vaughan-Jones et al., 2009; Wang et al., 2014), resulting in untoward accumulation of intracellular H^+(Casey et al., 2010; Vaughan-Jones et al., 2009). An unregulated decline of pH_i in the heart leads to reduced contractility, deranged Ca^{2+} signaling, and arrhythmias(Vaughan-Jones et al., 2009). Thus, the precise homeostatic control of cardiac pH is critical for normal cardiac function.

Studies have shown that acid-extruders, such as Na^+/H^+ exchanger (NHE) and Na^+-HCO_3^- cotransporter (NBC), as well as acid-loaders, like Cl^-/HCO_3^- (CBE) and Cl^-/OH^- (CHE) exchangers, mediate cardiac pH_i regulation(Vaughan-Jones et al., 2009). Methods for cardiac pH_i measurement have continued to evolve since the early 1960s ranging from the use of open-tipped glass micropipette electrodes, 5,5 dimethyl-2,4-oxazolidinedione (DMO), isotopes, pH-sensitive microelectrodes, nuclear magnetic resonance, and fluorescent dyes (Bers and Ellis, 1982; Blank et al., 1992; Ellis and Thomas, 1976a; 1976b; Hunjan et al., 1998; Kirschenlohr et al., 1988; Lavallee, 1964; Schroeder et al., 2010; Valkovic et al., 2019; Waddell and Bates, 1969). Cardiac pH_i was documented to range between 7 and 7.3 when HCO_3^- was used as the buffer. Due to the relatively large size of cardiomyocytes, compartmentalization of cellular activities causes spatial pH_i non-uniformity, and a pH_i gradient of up to ~0.1 unit was previously reported (Swietach and Vaughan-Jones, 2005b; Vaughan-Jones et al., 2006), suggesting that there exists a relatively weak coupling of pH_i and H^+-equivalent transporters with local regulatory mechanisms of pH_i. A recent study using confocal line-scan mode recorded ~3.6 nM proton concentration changes in the cytosol, which resulted from acid-yielding ATP hydrolysis during cardiomyocyte contraction (Hulikova and

[1]Department of Internal Medicine, University of California, Davis, Davis, CA 95616, USA

[2]Department of Pharmacology, University of California, Davis, Davis, CA 95616, USA

[3]Department of Physiology and Cell Biology, University of Nevada, Reno, Reno, NV 89557, USA

[4]Department of Biomedical Engineering, University of California, Davis, Davis, CA 95616, USA

[5]Department of Veterans Affairs, Northern California Health Care System, Mather, CA 95655, USA

[6]Lead contact

*Correspondence: xdzhang@ucdavis.edu

https://doi.org/10.1016/j.isci.2021.103624

Swietach, 2016). However, it remains unknown how the pH_i is regulated to match the beat-to-beat contraction of the heart.

We hypothesize that cardiac pH_i may experience beat-to-beat changes resulting from the burst of myofilament ATPase activity and rhythmic metabolic events, dampened by endogenous pH_i buffering. Results from simultaneous measurement of pH_i and sarcomere lengths demonstrate unequivocally that cardiac pH_i experiences beat-to-beat dynamic changes, termed"pH_i transients." The pH_i transients are coupled to cardiomyocyte contraction and regulated by pacing rate, sarcolemmal Cl^-/HCO_3^- transporters, pH_i buffering capacity, and β-adrenergic signaling. Inhibiting the mitochondrial electron transport chain (ETC) activities attenuates the pH_i transients suggesting the possible contributions of mitochondria in generating pH_i transients. Indeed, the beat-to-beat dynamic changes in pH_i during cardiac contraction reflect a rhythmic metabolic status in cardiomyocytes. We propose that temporal pH_i acidification may provide a transient increase in the driving force for H^+ transport to enhance mitochondrial ATP synthesis during cardiac contraction to meet the increased energy demand. Moreover, a decrease in pH_i may serve as a negative feedback to control the cardiac contraction due to the inhibitory effects on the contractile machinery by low pH_i. Our findings reveal a dynamic pH_i regulatory system in the heart that dovetails with the prevailing dynamic electrical, Ca^{2+}, and mechanical regulatory systems and have critical physiological and disease ramifications.

RESULTS

Intracellular pH in cardiomyocytes experiences dynamic beat-to-beat changes

Simultaneous pH_i and sarcomere lengths were measured and quantified in single ventricular cardiomyocytes during the contraction–relaxation cycle. To ensure that the changes in fluorescence signals were not due to motion artifacts, we positioned the relaxed cardiomyocyte within the imaging frame to capture the fluorescence signals from the whole cells. Moreover, two different fluorescent indicators including pHrodo green, an intensity-based pH dye, and SNARF-1, a ratiometric pH dye, were used to verify the results. Indeed, the pH_i in cardiomyocytes experiences dynamic beat-to-beat changes coupled with the contraction, termed pH_i transients (Figures 1A, and S2). Mouse and rabbit left ventricular myocytes were loaded with pHrodo green dye, bathed in HCO_3^--buffered Tyrode's solution and paced at 0.5 Hz (Figure 1A. Left: rabbit; Right: mouse). A significant acidification of pH_i was observed in response to each sarcomere contraction. For comparisons of the time courses of the pH_i and sarcomere contraction, ten cycle average traces of simultaneous pH_i and sarcomere length were overlayed and shown in the lower panel.

To further ensure that the pH_i transient observed was not due to motion artifacts or dependent on a specific pH dye, SNARF-1, a ratiometric dye was used to verify the findings. The major advantage of the ratiometric dye is the fact that it is less prone to motion artifacts from cell contractions. Similar dynamic beat-to-beat pH_i changes were observed using SNARF-1 (Figure 1B. Left: rabbit; Right: mouse; and Figure S2). The baseline pH_i is summarized in Figure 1C, together with the absolute pH_i transient amplitude (ΔpH_i) in Figure 1D. The baseline pH_i measured in mouse and rabbit cardiomyocytes using pHrodo green and SNARF-1 was similar; however, the pH_i transient amplitude in the mouse was significantly smaller than that in the rabbit cardiomyocytes (Figure 1D). Thus, we choose rabbit cardiomyocytes and use pHrodo green for subsequent studies.

We further measured pH_i and sarcomere length at physiological temperature (36°C) and pacing rate (1 Hz) in rabbit ventricular myocytes shown in Figure 1E. The baseline pH_i is significantly lower compared to that at RT (Figure 1F), and the absolute amplitude of pH_i transient at physiological temperature is significantly larger than that at RT (Figure 1G).

We analyzed the kinetics of the beat-to-beat pH_i changes in rabbit cardiomyocytes recorded at RT. The time-to-peak of the pH_i transient was 489 $\pm$ 28 ms (N = 7, n = 21. N represents animal numbers, while n represents cell numbers), while the time to the peak velocity was 112 $\pm$ 16 ms (n = 21). The recovering phase of the pH_i transient was fitted with a single exponential function with a time constant of 293 $\pm$ 24 ms (N = 7, n = 21). Additionally, the time-to-peak of the contraction (time to the maximum contraction or the shortest sarcomere length) was 524 $\pm$ 24 ms (N = 7, n = 21), which is not significantly different from that of the pH_i transient (489 $\pm$ 28 ms). In contrast, the time-to-peak contraction velocity (time to the maximum sarcomere contraction speed) was 45 $\pm$ 3 ms (N = 7, n = 21), which was significantly shorter than that of the pH_i transient ($p = 0.00034$). The relaxation phase of the contraction was well fitted by a single exponential function with a time constant of 203 $\pm$ 19 ms (N = 7, n = 21), which was significantly smaller than that of the pH_i transient (293 $\pm$ 24 ms) ($p = 0.0057$). The kinetic analyses support the coupling of the

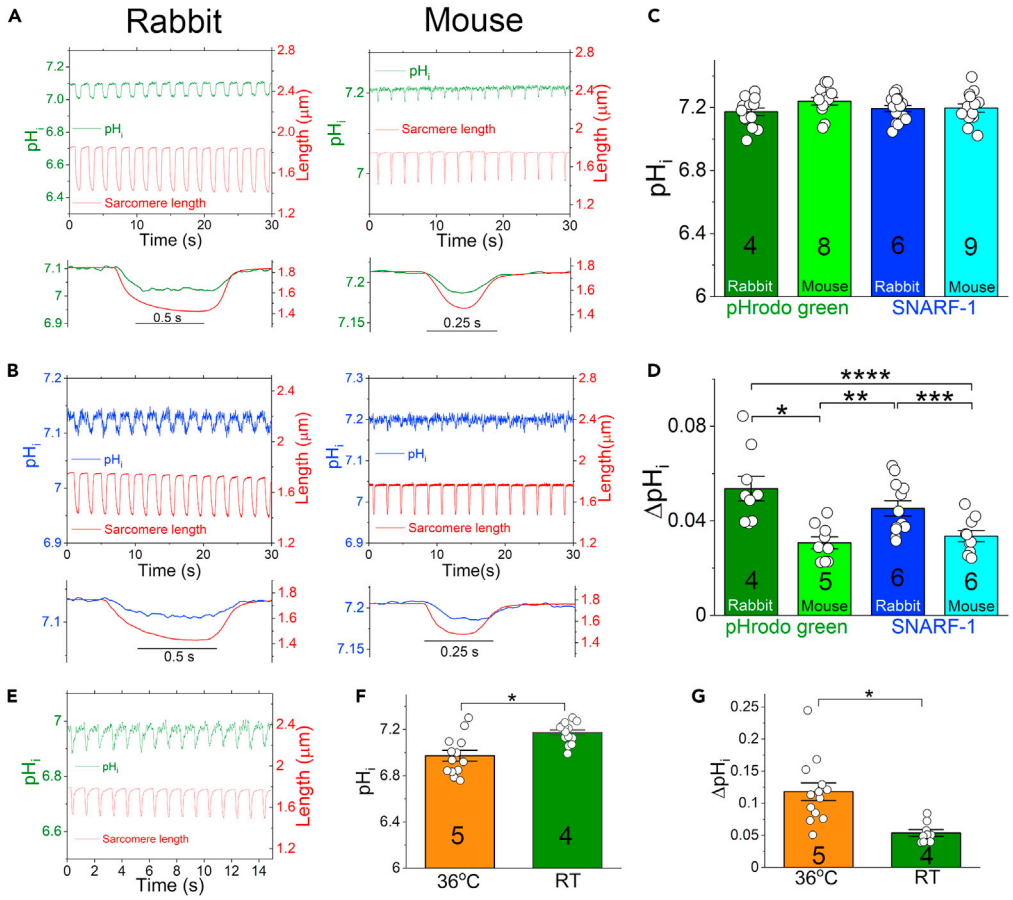

Figure 1. pH_i transients in rabbit and mouse ventricular cardiomyocytes recorded at RT and 36°C

(A) Representative traces of pH_i in rabbit (left) and mouse (right) ventricular myocytes in parallel with the sarcomere length measurement at RT. Cardiomyocytes were paced at 0.5 Hz with pHrodo green loading. The averaged traces of pH_i and sarcomere shortening are overlapped and shown in the lower panel.

(B) Representative traces of pH_i in rabbit (left) and mouse (right) ventricular myocytes in parallel with the sarcomere length measurement at RT. Cardiomyocytes were paced at 0.5 Hz with SNARF-1 loading. The averaged traces of pH_i and sarcomere shortening are overlapped and shown in the lower panel.

(C) Comparisons of the baseline pH_i measured at RT in rabbit (n = 14 and 16 for pHrodo green and SNARF-1, respectively) and mouse cardiomyocytes (n = 13 and 14 for pHrodo green and SNARF-1, respectively). Animal numbers (N) are shown in the bar graphs.

(D) Comparisons of the absolute pH_i transient amplitudes (ΔpH_i) in cardiomyocytes using pHrodo green (rabbit: n = 9, mouse: n = 9; *p = 0.010), and SNARF-1 (rabbit: n = 12, mouse: n = 10; **p = 0.012; ***p = 0.028, ****p = 0.021) at RT (one-way ANOVA combined with Tukey's post hoc analyses), where n represents cell numbers.

(E) pH_i measurement in rabbit ventricular myocytes using pHrodo green with simultaneous sarcomere length measurement paced at 1 Hz at 36°C.

(F and G) Comparisons of baseline pH_i (F, n = 14 and 13 for RT and 36°C, respectively; *p = 0.00069) and ΔpH_i (G, n = 9 and 13 for RT and 36°C, respectively; *p = 0.0014) in rabbit ventricular myocytes (two-sample *t* test). Data are represented as mean ± SEM.

See also Figures S2 and S3.

pH_i transient to the sarcomere contraction with a similar time-to-peak. However, the nearly 50% slower decay for the pH_i transient versus relaxation supports the notion that the signal is not likely a motion artifact. Indeed, if the pH_i transients reflect rapid ATP consumption, it is probable that the pH_i recovery may take longer than relaxation. In mouse cardiomyocytes, the time-to-peak of the pH_i transient was 170 ± 16 ms (N = 6, n = 15), which is significantly smaller than that of rabbit ($p = 1.7 \times 10^{-9}$); the time constant of mouse pH_i transient recovering phase was 143 ± 15 ms (N = 6, n = 15), which is also significantly smaller

than that of rabbit ($p = 0.000052$). The differences in the kinetics may be related to differential myosin subtypes in adult rabbit (β-myosin) and mouse (α-myosin) cardiomyocytes.

We did not find significant differences in the pH_i transients between the male and female mice (Figure S3A). In both mouse and rabbit atrial myocytes, the baseline pH_i is significantly lower than that in left ventricular myocytes, and the absolute amplitude of pH_i transients is larger than that in left ventricular myocytes (Figure S3B). We further examined the rabbit left and right ventricular myocytes, and we did not find significant differences in baseline pH_i and pH_i transients between rabbit left and right ventricular myocytes (Figure S3C).

Inhibition of cardiac contraction reduces the intracellular pH transient

To generate a cardiac contraction, coupled electrical and mechanical activities, as well as Ca^{2+} signaling and myofilament ATP hydrolysis, are required. ATP hydrolysis results in the acidification of pH_i. Moreover, mechanical activities alter the metabolic states of cardiomyocytes and activate mechanosensitive ion channels and transporters. These events are also expected to change the pH_i.

To decipher the underlying mechanisms for the observed beat-to-beat pH_i transients, we separate myofilament ATP consumption from ionic fluxes and other cellular events by taking advantage of a myosin ATPase inhibitor blebbistatin (BLEB, 25 μM) (Kovacs et al., 2004). Figure 2A shows that BLEB reduces the sarcomere contractions and causes a significant reduction of pH_i transient accompanied by an acidification of baseline pH_i. Example traces before (control), during (BLEB), and after (washout) of BLEB are shown in the right three panels in Figure 2A. Summary of the changes in baseline pH_i and the absolute amplitude of pH_i transients are shown in Figure 2C. Upon washout, the baseline pH_i and pH_i transients recovered slowly accompanied by partial recovery of the sarcomere contraction, suggesting partially reversible inhibitory effects of BLEB.

To further investigate the contraction-coupled pH_i transients, we applied another excitation–contraction (E–C) uncoupler, 2,3-butanedione 2-monoxime (BDM, 10 mM), to inhibit the contraction of cardiomyocytes(Backx et al., 1994). BDM significantly inhibited the contraction of cardiomyocytes as well as the pH_i transients (Figure 2B), but did not significantly affect the baseline pH_i (Figure 2D). Example traces before (control), during (BDM), and after (washout) BDM application are shown in the right three panels. The effect of BDM was reversible upon washout. We further tested the inhibitory effect of BDM in physiological conditions, and the results are similar to those obtained at RT as shown in Figure S4.

The observed significant reduction of pH_i transients suggests that the pH_i transient is coupled to the contraction of cardiomyocytes, and may result, in part, from the myofilament ATP hydrolysis.

Regulation of intracellular pH transients by intracellular pH buffering capacity

pH_i in cardiomyocytes is tightly regulated in normal cardiac function. However, in the pathological condition such as ischemia, the pH_i falls significantly in the infarcted myocardium (Vaughan-Jones et al., 2009). Moreover, respiratory or metabolic acidosis or alkalosis results in significant alterations in systemic pH as well as cardiac pH_i (Walley et al., 1990). To test the cellular mechanisms underlying the pH_i transients, we kept extracellular pH (pH_o) constant, but altered the pH_i by including sodium acetate or NH_4Cl in the bath solutions as previously described (Roos and Boron, 1981; Sirish et al., 2017; Thomas, 1984). We recorded pH_i transients and sarcomere lengths during the application of NH_4Cl and acetate as shown in Figure 3. Perfusion by NH_4Cl containing solutions significantly increased the baseline pH_i and enhanced the sarcomere contraction, but reduced the pH_i transients (Figures 3A and 3C). In contrast, inclusion of acetate significantly decreased the baseline pH_i, reduced the contraction but increased the pH_i transients (Figure 3B and 3D). These findings demonstrate that amplitudes of pH_i transients are decoupled from the sarcomere contraction when the baseline pH_i was altered, likely as a result of endogenous pH_i buffering capacity changes. Indeed, pH_i is critical in modulating the pH_i transients, providing an important regulatory mechanism of pH_i transients in physiological and pathological conditions.

Regulation of intracellular pH transients by extracellular HCO_3^- and Cl^-

The pH_i in cardiomyocytes is tightly regulated by a group of ionic transporters, including acid-extruders and acid-loaders. NHE and NBC mediate acid extrusion, while CBE and CHE mediate acid loading

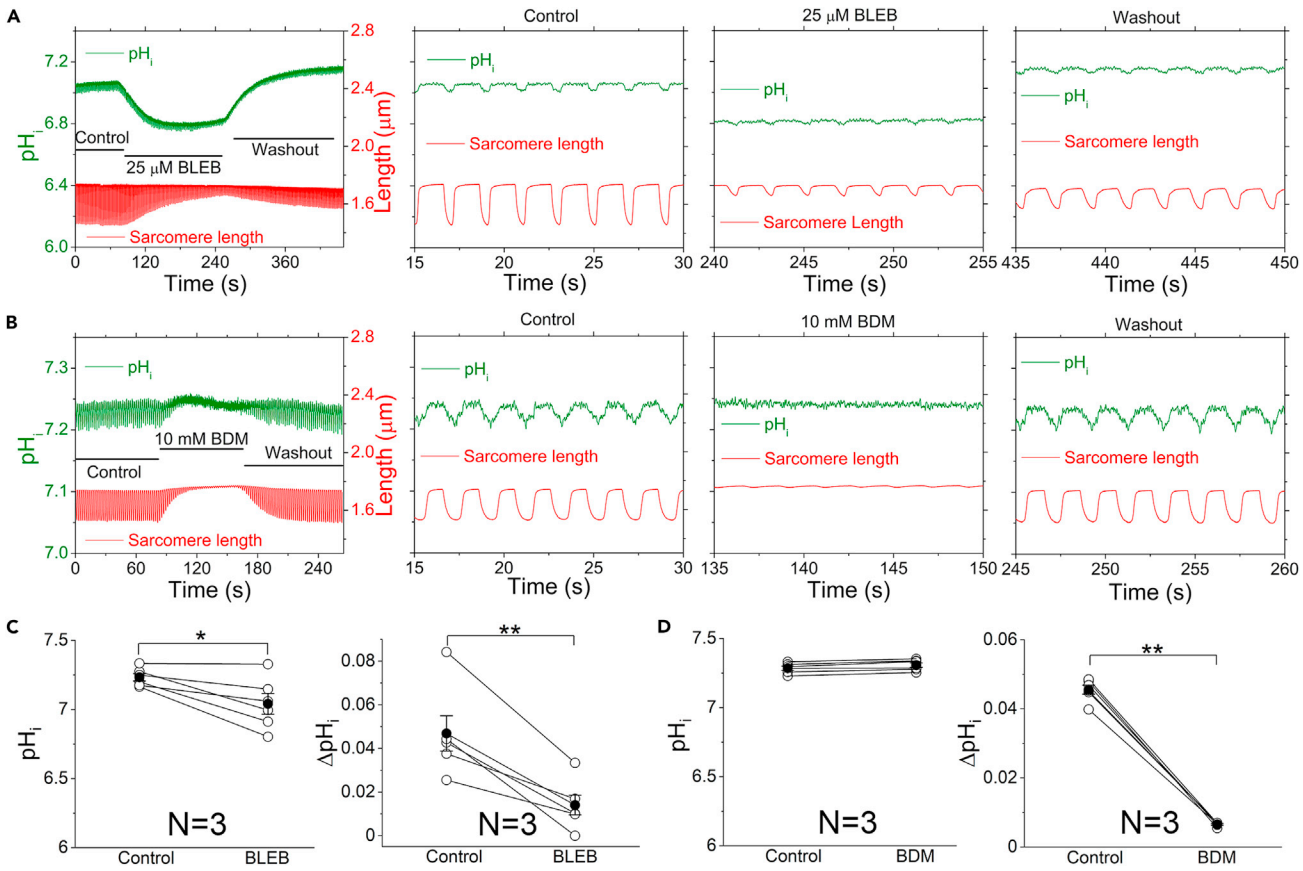

Figure 2. Reduction of pH_i transients by the inhibition of cardiomyocyte contractions

(A) Inhibition of the contraction by 25 μM BLEB reduced the pH_i transients.

(B) Inhibition of the contraction by 10 mM BDM abolished the pH_i transients. The right three panels in A and B showed three fragments of the time course at three conditions as shown on the top.

(C) Comparisons of baseline pH_i (*p = 0.0074, n = 6, paired sample *t* test) and ΔpH_i (**p = 0.0009; n = 6, paired sample *t* test) in the absence and presence of 25 μM BLEB.

(D) Comparisons of baseline pH_i and ΔpH_i in the absence and presence of 10mM BDM (**p = 0.0055, n = 6; paired sample *t* test). The open circles represent the individual data points, and the filled circles and the error bars represent Mean ± S.E.M. N and n represent the animal numbers and cell numbers, respectively.

See also Figure S4.

(Vaughan-Jones et al., 2009). Because of the acidification of pH_i transients during cardiac contractions, we hypothesize that acid loaders might play important roles in the regulation of pH_i transients. We, therefore, tested the effects of Cl^- and HCO_3^- on cardiac pH_i and contractions. We compared the effects of HEPES-buffered with that of HCO_3^--buffered Tyrode's solutions as shown in Figure 4A. After switching the perfusate from HCO_3^-- to HEPES-buffered solution, the baseline pH_i increased significantly, accompanied by an enhancement of the contraction. However, the amplitude of the pH_i transient was significantly reduced (Figure 4A). The exposure to the HEPES-buffered solution gradually reduced the contraction and pH_i transients (Figure 4D). This observation supports the significant role of HCO_3^- and HCO_3^- transporters in regulating the baseline pH_i, pH_i transients, and contractions. The acute alkalinization induced by HEPES-buffered solution is likely due to intracellular HCO_3^- combining with a proton and leaving the cell as CO_2. The baseline alkalinization decreases the intrinsic buffering capacity in HEPES-buffered solution (Leem et al., 1999); however, the pH_i transients were reduced likely as a result of the smaller contraction.

As CBE functions as an acid-loader, we predict that the reduction of extracellular Cl^- will reverse the direction of Cl^-/HCO_3^- exchange and increase the baseline pH_i. Thus, we tested the effects of extracellular Cl^- on the pH_i transient and contractions (Figure 4B). To reduce the Cl^- concentration, NaCl was replaced by an equal concentration of Na-Glutamate in HCO_3^--buffered solution. After switching the perfusate from

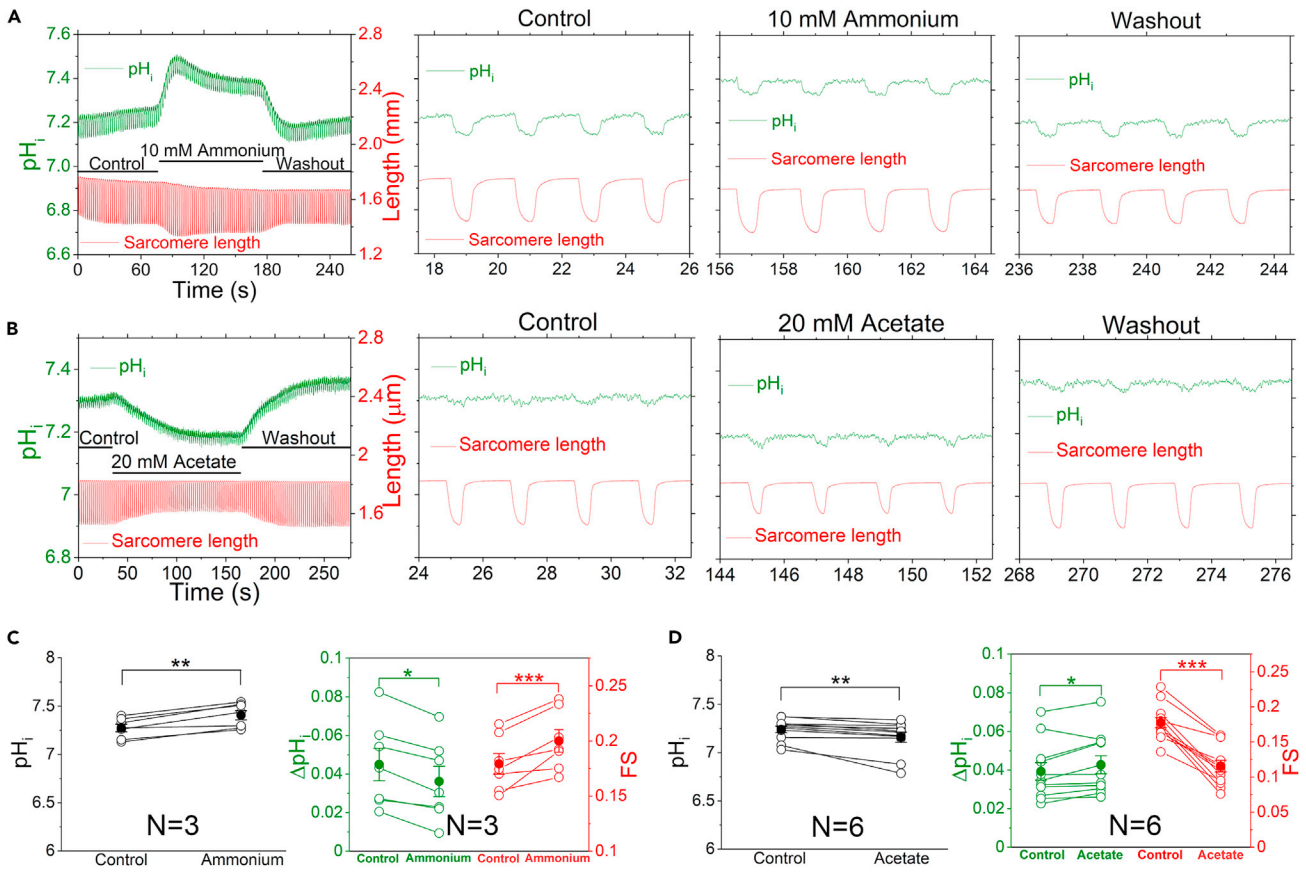

Figure 3. Regulation of pH_i transients by alterations of pH_i

(A) Effects of cellular alkalization by perfusing solutions containing 10 mM ammonium.

(B) Effects of cellular acidification by perfusing solutions containing 20 mM acetate. The right three panels in A and B showed three fragments of the time course at three conditions as shown on the top.

(C) Comparisons of baseline pH_i, ΔpH_i and sarcomere fractional shortening (FS) in the absence and presence of 10 mM ammonium (*p = 0.00072, **p = 0.00078, ***p = 0.0042, n = 7; paired sample *t* test).

(D) Comparisons of pH_i, ΔpH_i and FS in the absence and presence of 20 mM acetate (*p = 0.036, **p = 0.00098, ***p = 0.000028, n = 11; paired sample *t* test). N and n represent animal numbers and cell numbers, respectively. Data are represented as mean ± SEM.

high Cl^- (130 mM) to low Cl^- (10 mM) solution, the baseline pH_i increased significantly, accompanied by a slight reduction in contractions. Additionally, the pH_i transient was significantly reduced (Figures 4B and 4E). The findings support the roles of Cl^-/HCO_3^- exchangers in the regulation of baseline pH_i and pH_i transients, consistent with the results shown in Figures 3A and 4A. We further tested the role of NHE, an acid extruder, on pH_i transients using 10 μM EIPA, a specific inhibitor of NHE(Masereel et al., 2003). EIPA did not alter the baseline pH_i or pH_i transients significantly, suggesting negligible contributions from NHE at physiological pH_i (Figures 4C and 4F).

Regulation of intracellular pH transients by the beating rate of cardiomyocytes

The mechanical activities of cardiomyocytes are fueled by cardiac metabolism, which may contribute to the pH_i transients. Heart rates significantly alter cardiac metabolic demand and affect cardiac contractions. As pH_i transients are linked to the contraction, we reason that the beating rate of cardiomyocytes may alter the myofilament ATPase activity as well as the pH_i transients. We recorded pH_i transients from cardiomyocytes paced at 0.1, 0.5, 1, 2, and 4 Hz (Figure 5A). As the beating rate was increased, the sarcomere length in diastole shortened. The amplitude of contractions was reduced and the corresponding pH_i transient was decreased with increasing pacing rates (Figure 5B). The relationship between the time-averaged sarcomere length and the time-averaged pH_i at different pacing rates is shown in Figure 5C. The time-averaged sarcomere lengths represent the shortening of the myocytes during contraction as well as the diastolic

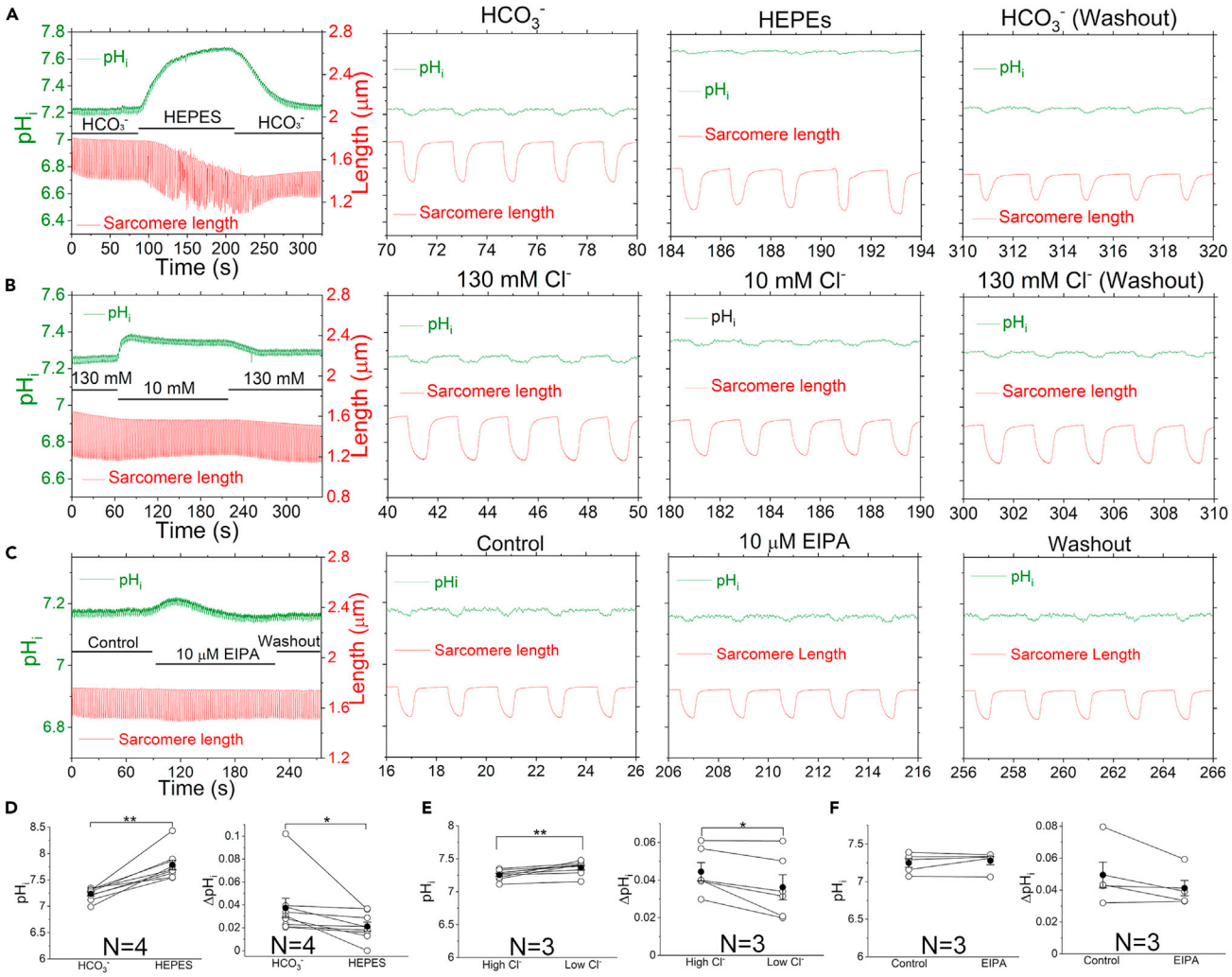

Figure 4. Effects of sarcolemma H^+-equivalent transporter activities on baseline pH_i and pH_i transients

(A) The time course of pH_i measurement when the cell was perfused with Tyrode's solutions either using HCO_3^- or HEPES as pH buffer (left).

(B) The time course of pH_i measurement when the cell was perfused with Tyrode's solutions containing higher (130 mM) and lower (10 mM) Cl^- (left).

(C) The time course of pH_i measurement when the cell was perfused by Tyrode's containing 10 μM EIPA (left). The right three panels in A, B, and C showed three fragments of the time course at three conditions as shown on the top of the panel.

(D) Comparisons of baseline pH_i and ΔpH_i of A (*p = 0.0039, n = 8; **p = 0.0039, n = 9; paired Wilcoxon signed-rank test).

(E) Comparisons of baseline pH_i and ΔpH_i of B (*p = 0.022, n = 6; **p = 0.0046, n = 9; paired sample *t* test).

(F) Comparisons of baseline pH_i and ΔpH_i of C (n = 5). N and n represent animal numbers and cell numbers, respectively. Data are represented as mean ± SEM.

sarcomere lengths as the relaxation is incomplete at higher rates (Figures 5A and 5C). Hence, the time-averaged sarcomere lengths reflect the averaged force, an index of ATP consumption rate (Brandes and Bers, 1996, 1997). With higher pacing rates, the time-averaged sarcomere length became shorter, consistent with higher averaged ATP consumption (and protons produced) and the lower averaged pH_i (Figure 5C). Figure 5D quantifies the amplitude of the steady-state sarcomere shortening (ΔSarcomere length) including the residual diastolic shortening against the amplitude of the pH_i transients (ΔpH_i). Similar to Figure 5C, the plot in Figure 5D also accounts for the progressive diastolic shortening at higher frequency. However, ΔpH_i was reduced with increased ΔSarcomere length (including the residual diastolic shortening) at higher pacing frequencies with increased ATP consumption. This suggests that the higher averaged ATP consumption may not be the sole mechanism underlying the generation of pH_i transients. To support the physiological relevance and significance, we performed the pacing experiment at 36°C, and similar results were obtained shown in Figure S5. To exclude the time-dependent effects, cells were returned to the lower

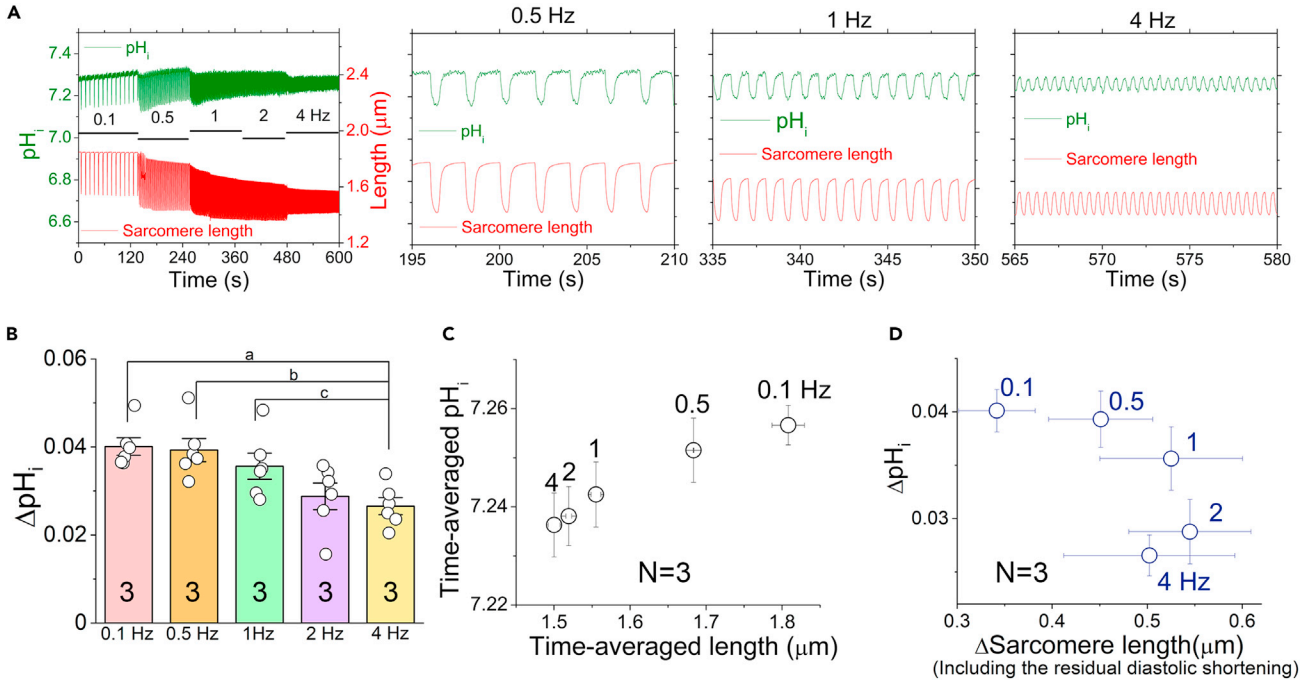

Figure 5. Increasing the pacing rate reduced the pH_i transients

(A) The time course of pH_i measurement was shown on the left, and the right three panels showed three fragments of the time course at three pacing rates.

(B) Comparisons of ΔpH_i at different pacing rates (The p values for a: 0.018; b: 0.0087; c: 0.01. n = 6, one-way repeated measures ANOVA combined with Tukey's post hoc analyses). Animal numbers (N) are shown in the bar graphs.

(C) The relationship between the time-averaged sarcomere length and the time-averaged pH_i during pacing at different pacing rates (n = 6).

(D) The relationship between ΔpH_i and ΔSarcomere length (including the residual diastolic shortening) at different pacing rates (n = 6). N and n represent animal numbers and cell numbers, respectively. Data are represented as mean ± SEM.

See also Figures S5 and S6.

pacing rate after pacing at high rates. There was a significant recovery of the baseline pH_i and pH_i transients upon returning to the lower pacing rate (Figure S6).

Activation of β-adrenergic signaling increases the intracellular pH transient

Acute activation of β-adrenergic signaling induces positive inotropic effects on cardiac myocyte contraction. Submicromolar isoproterenol was previously documented to be effective to increase intracellular Ca^{2+} levels (Zou et al., 2001). Figure 6A shows the effects of 50 nM isoproterenol on the contraction and pH_i transients. Isoproterenol stimulated a brief transient alkalization of baseline pH_i and a more gradual rise in the amplitude of contraction and pH_i transients. Figure 6C shows significant increases in both myocyte contractions and pH_i transients after isoproterenol stimulations. The findings reflect the increase in averaged force and thus, an index of energy consumption rate and pH_i transients. In contrast, Ca^{2+} channel blocker, verapamil, has negative inotropic effects on cardiac contractions (Bell and McDermott, 1995; Kanaya et al., 2006). We further tested the effects of verapamil on cardiac contractions and pH_i transients. Figures 6B and 6D demonstrate the inhibitory effects of 2.5 μM verapamil on the contraction, with reduced pH_i transients and elevated baseline pH_i in rabbit cardiomyocytes.

Inhibiting mitochondrial electron transport chain reduces the intracellular pH transients

Mitochondria are the powerhouse for cardiomyocytes, and the generation of an H^+ gradient across the inner mitochondrial membrane is essential for ATP synthesis. We hypothesize that in addition to beat-to-beat ATP hydrolysis and energy consumption, the pH_i transients may also be coupled to the mitochondrial H^+ transfer driving the mitochondrial ATP synthesis. Therefore, we applied different inhibitors to probe the functional impacts of the mitochondrial ETC on the baseline pH_i and pH_i transients.

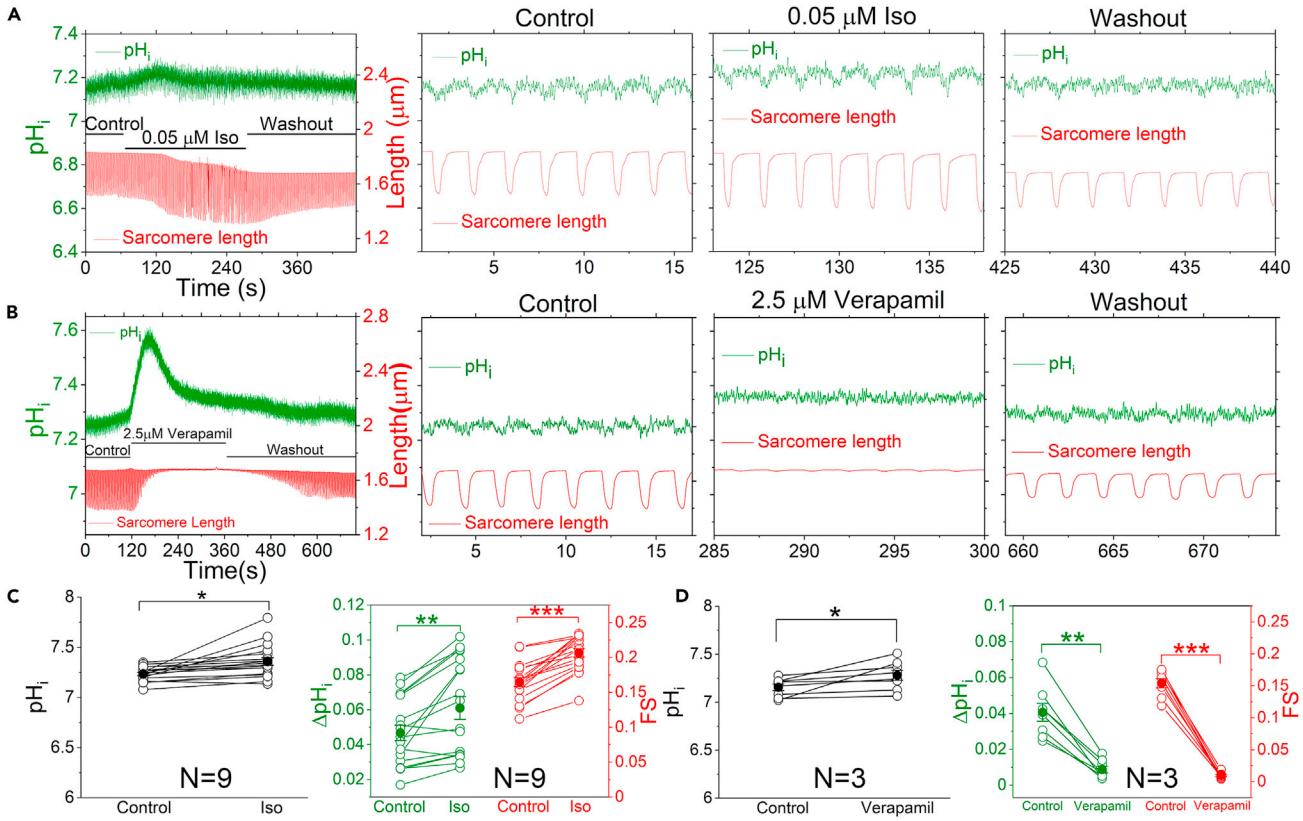

Figure 6. Activation of β-adrenergic signaling by isoproterenol increased the pH_i transients

(A) The time course of pH_i measurement with the perfusion of Tyrode's solutions containing 0.05 μM isoproterenol (Iso) was shown on the left, and the right three panels showed three fragments of the time course at three conditions.

(B) The time course of pH_i measurement with the perfusion of Tyrode's solutions containing 2.5 μM verapamil was shown on the left, and the right three panels showed three fragments of the time course at three conditions.

(C) Comparisons of baseline pH_i (*p = 0.0024, n = 18), ΔpH_i and sarcomere fractional shortening (FS) (**p = 0.00084, n = 18; ***p = 0.0000076, n = 18) in the absence and presence of 0.05 μM of isoproterenol (paired sample *t* test).

(D) Comparisons of baseline pH_i (*p = 0.035, n = 8), ΔpH_i and FS (**p = 0.00010, n = 8; ***p = 0.00000017, n = 8) in the absence and presence of 2.5 μM of verapamil (paired sample *t* test). N and n represent animal numbers and cell numbers, respectively. Data are represented as mean ± SEM.

Rotenone and antimycin A (Wiersma et al., 2019), which inhibit complex I and III, respectively, reduce proton pumping out of the matrix, which is expected to cause cytosolic alkalinization. Indeed, either inhibitor acutely alkalinized the baseline pH_i, reduced the pH_i transient, and increased contractions (Figures 7A, 7B, 7D, and 7E). The increased contractility likely results from pH_i alkalization, and as the alkalinization subsided contractility declined. Finally, we examined the effect of 2-[2-[4-(trifluoromethoxy) phenyl] hydrazinylidene]-propanedinitrile (FCCP) (Bassani et al., 1992; Neary et al., 2014; Thai et al., 2018), a protonophore and an uncoupler of the ETC on pH_i. Although FCCP initially allows mitochondrial H^+ entry (transiently alkalinizing the cytosol), the uncoupling results in ATP synthase reversal as a major futile ATPase that generates acid decreasing the pH_i. Indeed, FCCP acidified baseline pH_i, abolished contractions, and hence abolished the pH_i transient associated with the contraction (Figures 7C and 7F). A summary diagram in Figure 7G illustrates the beat-to-beat pH_i regulatory system that dovetails with the prevailing dynamic electrical, Ca^{2+}, and mechanical regulatory systems.

DISCUSSION

Cardiac function is shaped by three tightly coupled dynamic systems, including electrical excitation, Ca^{2+} signaling, and mechanical contraction. Our study identifies a dynamic beat-to-beat pH_i system in the heart, that is tightly coupled with the other three dynamic systems due to the exquisite effects of pH_i on cardiac excitability, Ca^{2+} signaling, and contractions(Vaughan-Jones et al., 2009).

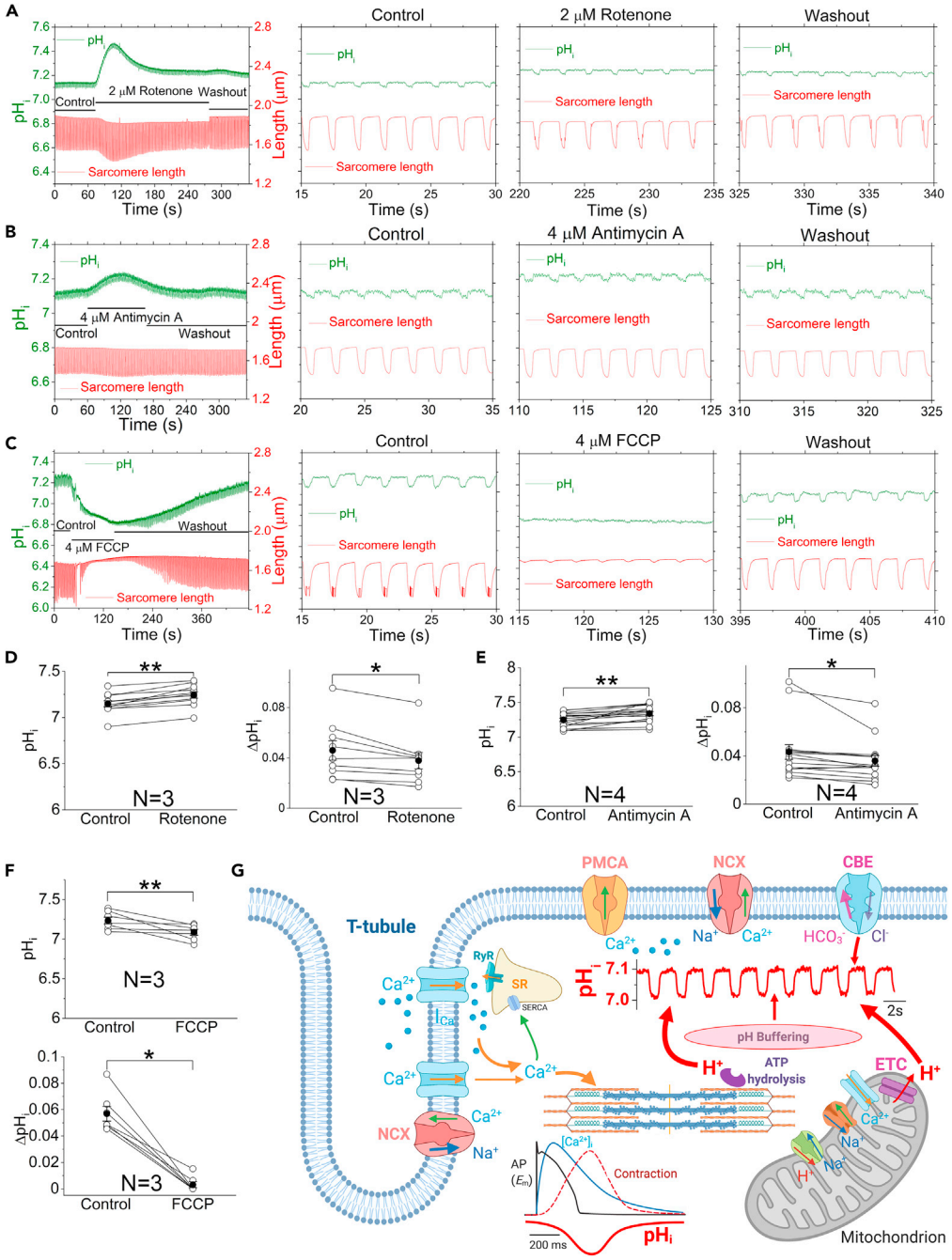

Figure 7. Inhibition of mitochondrial ETC reduced the pH_i transients

(A–C) Time courses of pH_i measurement when the cell was perfused by Tyrode's containing 2 μM rotenone (A, left), or containing 4 μM antimycin A (B, left), or containing 4 μM FCCP (C, left). The right three panels showed three fragments of the time course at three conditions as shown on the top.

(D) Comparisons of baseline pH_i (**p = 0.000083, n = 11, paired sample *t* test) and ΔpH_i of A (*p = 0.0078, n = 9; ΔpH_i: 0.046 ± 0.008 in control vs 0.038 ± 0.006 with rotenone, paired Wilcoxon signed-rank test). After washout, ΔpH_i = 0.045 ± 0.007, and is not statistically different compared to control (p = 0.86).

(E) Comparisons of baseline pH_i (**p = 0.00056, n = 17, paired sample *t* test) and ΔpH_i of B (*p = 0.00031, n = 15. ΔpH_i: 0.046 ± 0.007 in control vs 0.037 ± 0.006 with antimycin A, paired Wilcoxon signed-rank test). After washout, ΔpH_i = 0.045 ± 0.005, and is not statistically different compared to control (p = 0.67).

(F) Comparisons of baseline pH_i (**p = 0.0002, n = 7, paired sample *t* test) and ΔpH_i of C (*p = 0.016, n = 7, paired Wilcoxon signed-rank test. ΔpH_i: 0.057 ± 0.006 in control vs 0.003 ± 0.002 with FCCP). After washout, ΔpH_i = 0.055 ±

Figure 7. *Continued*

0.005, and is not statistically different compared to control (p = 0.63). N and n represent animal numbers and cell numbers, respectively. Data are represented as mean ± SEM.

(G) A summary diagram (created using BioRender.com) showing the beat-to-beat pH_i regulatory system that dovetails with the prevailing dynamic electrical, Ca^{2+}, and mechanical regulatory systems. SR: sarcoplasmic reticulum; RYR: ryanodine receptor; SERCA: sarcoplasmic reticulum Ca^{2+} ATPase; PMCA: plasma membrane Ca^{2+}-ATPase; NCX: Na^+/Ca^{2+} exchanger; AP: action potential; CBE: Cl^-/HCO_3^- exchanger; E_m: membrane potential; ETC: electron transport chain.

Cardiac intracellular pH is tightly and dynamically regulated

pH_i governs the ionization states of all weak acids and bases in the cell and plays critical roles in cellular function. Under physiological conditions, pH_i is relatively acidic compared to pH_o (~7.3–7.4) (Casey et al., 2010). Cardiomyocytes are vulnerable to pH_i changes as the molecules participating in the regulation of cardiac excitability and contractility such as ion channels, transporters, and contractile proteins are exquisitely sensitive to pH_i (Sirish et al., 2017; Thorsen et al., 2017; Vaughan-Jones et al., 2009; Wang et al., 2014). In pathological conditions such as myocardial ischemia, a large fall of pH_i (~6.5) occurs, resulting in depressed cardiac contractility, abnormal intracellular Ca^{2+} signaling, and arrhythmias (Garlick et al., 1979; Steenbergen et al., 1977; Vaughan-Jones et al., 2009). The mammalian heart beats incessantly with rhythmic and robust electrical and mechanical activities consuming ATP and generating acids. Even though the intrinsic and HCO_3^- mobile buffering capacity in cardiomyocytes is strong, there remain pH_i fluctuations and non-uniformity in cardiomyocytes. Fluctuations of pH_i may occur during changes in cardiac workload and heart rate (Bountra et al., 1988; Elliott et al., 1994; Vaughan-Jones et al., 2009). Previous studies demonstrate that there is a significant spatial non-uniformity in pH_i of cardiomyocytes, attributed to the low intracellular H^+ mobility (Swietach et al., 2005; Swietach and Vaughan-Jones, 2005a; 2005b; Vaughan-Jones et al., 2002; Vaughan-Jones et al., 2006). The heterogeneity of pH_i in cardiomyocytes suggests local regulatory machinery and spatial control of pH_i.

Cardiac pH_i measurement and regulation have been extensively investigated over the past several decades since the 1960s (Bers and Ellis, 1982; Blank et al., 1992; Ellis and Thomas, 1976a; 1976b; Hunjan et al., 1998; Kirschenlohr et al., 1988; Lavallee, 1964; Schroeder et al., 2010; Valkovic et al., 2019; Waddell and Bates, 1969). However, to eliminate the motion-induced instability for recordings by microelectrodes or reduce the motion distortion in confocal microscopic imaging, previous studies were performed mostly using quiescent cardiac tissues and cardiomyocytes. Furthermore, low temporal resolution limited the capture of the fast pH_i changes. A recent study explored the nuclear proton dynamics in rat cardiomyocytes and showed a ~3.6 nM increase in proton concentration (from 95.3 ± 0.002 to 99.0 ± 0.01 nM) in the cytosol along the long axis of the cell during contraction, and the index of contraction was shown by the width changes of the fluorescence signals. This measurement was performed using confocal line scan mode and the contraction of the cardiomyocytes was not directly quantified. The authors concluded that the small proton concentration change may result from acid-yielding ATP hydrolysis during cardiomyocyte contractions (Hulikova and Swietach, 2016).

Our study directly quantifies simultaneous changes of sarcomere length and pH_i during the cardiac cycle and documents a significantly larger increase in free H^+ concentration at RT and physiological conditions (36°C with 1 or 2 Hz pacing). The average value of pH_i transient amplitudes in rabbit cardiomyocytes is ~0.055 unit at RT or ~0.12 at 36°C, which corresponds to a free H^+ concentration increase of ~10 nM at RT or ~30 nM at 36°C from baseline pH_i of 7–7.2. The proton buffering power in cardiomyocytes is in the order of 20-90 mM per pH unit (Crampin et al., 2006). If we use a median value of 50 mM per pH unit for the calculation of the total H^+ release using the method previously reported(Hulikova and Swietach, 2016), 10 and 30 nM changes in free H^+ concentrations represent 2 and 6 mM changes in total H^+ concentrations, respectively. A previous study has shown that cooling from 37 to 27°C decreases both the intrinsic buffer power and acid extrusion from the cell, and the resting pH_i is ~0.1 pH units lower at 37°C(Ch'en et al., 2003). Our resting pH_i values measured at 36°C (6.97 ± 0.05, n = 13) and RT (7.17 ± 0.02, n = 14) are consistent with this previous finding (Ch'en et al., 2003). However, the absolute amplitude of pH_i transients is significantly larger at 36°C (0.12 ± 0.01, n = 13) than that at RT (0.055 ± 0.005, n = 9), suggesting that the buffering power is not the only regulatory factor for the pH_i transients.

To ensure that the recorded pH transients were not due to motion artifacts, we agonize over several important features in our recordings. First is to position the cells completely within the imaging frame during the recordings to capture fluorescence signals from the entire cell. Next, we use two different fluorescence indicators including pHrodo green and SNARF-1, a ratiometric dye, to directly verify the results. Additionally, we analyzed the time course of pH_i transients and sarcomere contraction to compare the kinetic parameters and coupling. The time to peak contraction velocity for sarcomere contraction was used to compare to the time to peak velocity of pH transients, revealing a significantly slower kinetics in pH_i transients than that of sarcomere contraction. Furthermore, data shown in Figure 3 provide clear evidence that pH_i transients can be decoupled with the sarcomere contraction. Specifically, the decreased pH_i transients were accompanied by enhanced contractions (Figure 3A) or *vice versa* (Figure 3B). Moreover, the immediate effect of the inhibition of ETC is the enhancement of contractions. However, this is accompanied by reduced pH_i transients (Figure 7A and 7B), illustrating the decoupled changes of contractions and pH_i transients, and providing further evidence that the pH_i transient does not result from the motion artifacts.

The differences of the pH_i transient amplitude between rabbit and mouse cardiomyocytes may result from the differential fractional shortening (FS) with significantly higher FS in rabbit cardiomyocytes (rabbit: 17 $\pm$ 1%, n = 19; mouse: 8 $\pm$ 2%, n = 12. p = 0.000022), as well as differences in the metabolic demands for cardiomyocyte contractions in rabbits and mice. The faster kinetics of pH_i transients in mouse cardiomyocytes may be due in part to the higher velocities of mouse α-myosin compared to rabbit β-myosin (Malmqvist et al., 2004).

The differences in baseline pH_i and pH_i transients between atrial and ventricular myocytes may result from distinct expression levels of H^+-equivalent transporters, metabolic profiles, and pH_i buffering capacity, which need to be further investigated.

Actions of 2,3-butanedione 2-monoxime and blebbistatin on intracellular pH transients

Both BDM and BLEB inhibit myofilament force production by binding to myosin. BLEB is a more specific inhibitor and binds to the motor domain of myosin II, while BDM is less specific with low affinity due to its inhibition of other myosins and its interactions with other proteins (Bond et al., 2013). Our results show that both inhibitors significantly reduce pH_i transients with simultaneous inhibition of contractions. BDM effect is reversible, while the BLEB effect is only partially reversible. However, the baseline pH_i decreases during the application of BLEB while the baseline pH_i remains the same upon the application of BDM, suggesting different mechanisms of BLEB and BDM in altering the ATP hydrolysis and metabolic status of cardiomyocytes. The effects of BLEB and BDM on pH_i demonstrated in our study suggest that alterations in pH_i need to be carefully considered in the result interpretations when these reagents are used in studies of E–C coupling.

Regulation of intracellular pH transients

The proton buffering capacity of the cell is governed by the protonated states of the buffers. In turn, the pH_i alters the protonated states of the buffers depending on the pK_a. The intrinsic buffer capacity varied inversely with pH_i, while the CO_2/bicarbonate buffering capacity increases monotonically with pH_i. As a result, the total buffering capacity increases with a rise of pH_i in CO_2/HCO_3^--buffered conditions (Leem et al., 1999). In our studies, we used CO_2/bicarbonate-buffered solutions during pH recordings. We demonstrate that the amplitudes of pH_i transients are significantly regulated by pH_i, with decreased pH_i transients by increased pH_i and *vice versa* (Figure 3). This highlights the effect of pH_i buffering capacity on pH_i transients. Lower extracellular Cl^- also causes intracellular alkalinization resulting in reduced pH_i transient, but the contraction is slightly inhibited, which needs to be further investigated. The alkalinization caused by lower extracellular Cl^- in our experiment is faster than that in sheep Purkinje fibers (Vaughan-Jones, 1979), which may result from the relatively slower solution penetration of Purkinje fibers and different recording methods. These results support the critical roles of membrane Cl^-/HCO_3^- exchangers in the regulation of pH_i transients. Cl^-/HCO_3^- exchangers may regulate pH_i transients by altering the baseline pH_i and the buffering capacity. On the other hand, inhibition of NHE did not significantly affect the pH_i, suggesting that NHE is not activated with neutral pH_i and, therefore, has no effects on pH_i transients.

A previous study using ion-selective microelectrodes reported that the increase in pacing rate causes the fall of baseline pH_i in sheep Purkinje fibers suggesting frequency-dependent intracellular acidosis (Bountra et al., 1988). Our data show cellular acidosis with higher pacing rates in rabbit ventricular myocytes consistent with the previous findings (Figures 5 and S5). However, the increase in pacing rates reduces the contraction amplitude and in turn, the pH_i transients. The increase in intracellular Ca^{2+} and Na^+ concentrations with higher pacing rates may affect the cell contraction. In addition, higher pacing rates reduce the time-averaged sarcomere length suggesting increased force and more ATP hydrolysis. The time-averaged sarcomere length represents cardiomyocyte shortening during a contraction that includes the diastolic sarcomere lengths, which reflects the averaged force and is an index of ATP consumption rate. We further evaluated the relationship between the amplitude of pH_i transients with the delta sarcomere length including the residual diastolic shortening (delta sarcomere length plus diastolic sarcomere length changes) (Figure 5D). Specifically, even though the delta sarcomere length is shorter at higher pacing frequency, the residual diastolic shortening is actually larger which indicated the higher ATP consumption rate. In this case, we observed an inverse relationship, that is, the amplitude of pH_i transients is reduced at higher pacing frequency, suggesting that ATP hydrolysis may not be the sole mechanism underlying the generation of pH_i transients. A possible factor that may affect the pH_i is the breakdown of phosphocreatine to restore ATP at higher pacing rate with increased workload (Zervou et al., 2016). The effect of increased pacing rates on pH_i transients is opposite to the effect of β-adrenergic signaling stimulation. The underlying mechanisms may involve different posttranslational modifications in the cellular calcium handling, sarcomeric proteins, rate-limiting steps in the SERCA transport cycle, and altered pH_i and mitochondrial function. Additionally, the biological function of isoproterenol on cardiomyocytes may not be limited to increased contractility. Isoproterenol also alters intracellular signaling by activating different protein kinases which may contribute to pH_i regulation. These will be further investigated in our future studies.

Role of mitochondria in generating intracellular pH transients

Mitochondria govern the metabolic and energetic status of cardiomyocytes. ETC in the inner membrane of mitochondria plays critical roles in ATP synthesis through oxidative phosphorylation. The central role of ETC is to establish the proton-motive force by generating an H^+ gradient across the inner membrane (Santo-Domingo and Demaurex, 2012). As the mitochondrial outer membrane is freely permeable to H^+, we expect a rapid equilibrium of H^+ with the mitochondrial intermembrane space. We demonstrate that the inhibition or uncoupling of ETC reduces or abolishes pH_i transients suggesting the possible contributions of mitochondria in the generation of pH_i transients. The inhibition of H^+ pumping into the intramembranous space causes cytosolic alkalinization and reduces the pH_i transients. The partial recovery phase from the rapid alkalinization caused by rotenone and antimycin A may stem from the compensatory mechanisms in the mitochondrial ETC. The mitochondrial uncoupler FCCP causes an increase of the respiration rates and cytosolic acidification with thermodynamically unrestrained H^+ pumping and possibly with the reverse-mode of ATP synthase which hydrolyzes ATP to generate acid, resulting in the cessation of pH_i transients and contractions. The elevation of mitochondrial Ca^{2+} is essential for controlling the ATP production to match cardiac demands during contractions (Bell et al., 2006; Dedkova and Blatter, 2013; Lu et al., 2013; Robert et al., 2001). Thus, pH_i transients in cardiomyocytes may report the dynamic beat-to-beat oscillations of mitochondrial H^+ transfer and bioenergetics that couple with the mitochondrial Ca^{2+} and mechanical signaling. The pH_i transients may provide a transiently increased H^+ driving force to enhance the ATP synthesis during cardiomyocyte contractions to meet the increased energy demand for contractions, suggesting a rhythmic metabolic status in cardiomyocytes. Taken together, H^+ transport across the mitochondrial inner membrane may play critical roles in the generation of pH_i transients in cardiomyocytes.

Physiological implications and future studies

Our study has important physiological implications. The pH_i transients in cardiomyocytes suggest the beat-to-beat dynamic regulation of mitochondrial function for ATP synthesis and myofilament ATP hydrolysis synchronize the energy production and consumption for contractions. Additionally, the acidification caused by pH_i transients during contractions may provide a negative feedback to the contractile elements, and facilitate the relaxation of cardiomyocytes due to the reduced cardiac contractility by low pH_i (Harrison et al., 1992; Orchard and Kentish, 1990; Vaughan-Jones et al., 2009). The effects of mitochondrial inhibitors are statistically significant; however, the biological relevance needs to be further investigated. In addition, many aspects of the cell function may affect the pH_i. Therefore, future experimental and computational

studies are required to further test the mechanisms of mitochondria and other cellular processes in the generation of pH_i transients, including real-time measurement of ATP production and consumption in cardiomyocytes as well as mathematical pH_i modeling.

Limitations of the study

ATP hydrolysis is accompanied by the release of H^+ with a stoichiometry coefficient less than 1 depending on pH_i and intracellular cation concentrations (Kushmerick, 1997); ATP synthesis also needs the proton transfer by mitochondrial ETC, and each ATP generated requires the transport of an estimated 4 protons (Turina et al., 2003). Therefore, ATP consumption and production will affect the total H^+ concentrations in cytosol, and they are one of the important mechanisms for dynamic pH_i regulation. Due to the complexity of the pH_i regulation system in the cells involving H^+ generation and buffering, H^+ transport, Ca^{2+} buffering and signaling, and other metabolic activities, it is difficult to quantitatively correlate pH_i transients with the ATP consumption and production in this study.

Additionally, although we optimized the experimental condition to load the dye to the cytosol, due to the dyes' intrinsic properties, we could not rule out the effects of the dye loading into intracellular organelles which may affect our results. To this end, saponin treatment was performed to quantify the dye loading, demonstrating specific cytosol loading in our experiments. Secondly, the fluorescent dye may be subjected to photobleaching and leakage, which may cause the baseline pH drift. To circumvent this effect, we have conducted control experiments to record the baseline signals which have been used for the correction of the pH measurement (Figure S1).

STAR★METHODS

Detailed methods are provided in the online version of this paper and include the following:

- KEY RESOURCES TABLE
- RESOURCE AVAILABILITY
  - Lead contact
  - Materials availability
  - Data and code availability
- EXPERIMENTAL MODEL AND SUBJECT DETAILS
- METHOD DETAILS
  - Cell isolation and chemicals
  - Measurement of pH_i and sarcomere length
- QUANTIFICATION AND STATISTICAL ANALYSIS

SUPPLEMENTAL INFORMATION

Supplemental information can be found online at https://doi.org/10.1016/j.isci.2021.103624.

ACKNOWLEDGMENTS

We thank Dr. Joe Soughayer from IonOptix for his support in the configuration and troubleshooting of the measurement system. This work was supported by NIH R56 HL138392 to X.D.Z, NIH R01 HL085727, HL085844, HL137228, and VA Merit Review Grant I01 BX000576 and CX001490 (N.C.), and additional support provided by NIH R01 HL123526 (Y.C.I.), NIH R01 HL081562 (D.M.B., J.B.), NIH R01 DC015135, AG051443, DC015252, DC016099, AG060504 (E.N.Y), and Postdoctoral Fellowship from NIH/NHLBI Institutional Training Grant in Basic and Translational Cardiovascular Science T32 HL086350, and NIH F32 HL149288 (P.N.T.), and American Heart Association (AHA) Predoctoral Fellowship Award 18PRE34030199 (L.R.). NC is the holder of the Roger Tatarian Endowed Professorship in Cardiovascular Medicine and a part-time staff physician at VA Northern California Health Care System, Mather, CA.

AUTHOR CONTRIBUTIONS

X.D.Z. proposed and developed the concept, designed the study, initially tested the concept by experiments, analyzed the data, made figures, and wrote the manuscript. N.C. helped with experiment design, data analysis and interpretation, and revised the manuscript; Y.L. performed the intracellular pH and contraction measurement, data analysis, and organization; P.N.T. and L.R. tested dye loading conditions, conducted part of the imaging experiment, and contributed to figure making; V.T. isolated the mouse

cardiomyocytes and contributed to the writing of STAR Methods; Z.J. isolated the rabbit cardiomyocytes; S.P. helped on the initial pH measurement experiments; K.S.G. and J.B. supervised the rabbit cell isolation, and K.S.G. contributed to the writing of STAR Methods and J.B. revised the manuscript; D.M.B. revised the manuscript and helped on the data analysis and interpretation; J.O. prepared and distributed the cardiomyocytes; Y.C.I. sponsored the rabbit cardiomyocyte isolation and revised the manuscript; E.N.Y. revised the manuscript and helped on the data acquisition and analysis.

DECLARATION OF INTERESTS

The authors declare no competing interests.

INCLUSION AND DIVERSITY

We worked to ensure sex balance in the selection of non-human subjects. One or more of the authors of this paper self-identifies as an underrepresented ethnic minority in science. One or more of the authors of this paper self-identifies as living with a disability.

Received: August 9, 2021
Revised: November 10, 2021
Accepted: December 10, 2021
Published: January 21, 2022

REFERENCES

Backx, P.H., Gao, W.D., Azan-Backx, M.D., and Marban, E. (1994). Mechanism of force inhibition by 2,3-butanedione monoxime in rat cardiac muscle: roles of [Ca2+]i and cross-bridge kinetics. J. Physiol. *476*, 487–500. https://doi.org/10.1113/jphysiol.1994.sp020149.

Bartos, D.C., Morotti, S., Ginsburg, K.S., Grandi, E., and Bers, D.M. (2017). Quantitative analysis of the Ca(2+) -dependent regulation of delayed rectifier K(+) current IKs in rabbit ventricular myocytes. J. Physiol. *595*, 2253–2268. https://doi.org/10.1113/JP273676.

Bassani, R.A., Bassani, J.W., and Bers, D.M. (1992). Mitochondrial and sarcolemmal Ca2+ transport reduce [Ca2+]i during caffeine contractures in rabbit cardiac myocytes. J. Physiol. *453*, 591–608. https://doi.org/10.1113/jphysiol.1992.sp019246.

Bell, C.J., Bright, N.A., Rutter, G.A., and Griffiths, E.J. (2006). ATP regulation in adult rat cardiomyocytes: time-resolved decoding of rapid mitochondrial calcium spiking imaged with targeted photoproteins. J. Biol. Chem. *281*, 28058–28067. https://doi.org/10.1074/jbc.M604540200.

Bell, D., and McDermott, B.J. (1995). Inhibition by verapamil and diltiazem of agonist-stimulated contractile responses in mammalian ventricular cardiomyocytes. J. Mol. Cell Cardiol. *27*, 1977–1987. https://doi.org/10.1016/0022-2828(95)90019-5.

Bers, D.M., and Ellis, D. (1982). Intracellular calcium and sodium activity in sheep heart Purkinje fibres. Effect of changes of external sodium and intracellular pH. Pflugers Arch. *393*, 171–178. https://doi.org/10.1007/bf00582941.

Blank, P.S., Silverman, H.S., Chung, O.Y., Hogue, B.A., Stern, M.D., Hansford, R.G., Lakatta, E.G., and Capogrossi, M.C. (1992). Cytosolic pH measurements in single cardiac myocytes using carboxy-seminaphthorhodafluor-1. Am. J. Physiol. *263*, H276–H284.

Bond, L.M., Tumbarello, D.A., Kendrick-Jones, J., and Buss, F. (2013). Small-molecule inhibitors of myosin proteins. Future Med. Chem. *5*, 41–52. https://doi.org/10.4155/fmc.12.185.

Bountra, C., Kaila, K., and Vaughan-Jones, R.D. (1988). Effect of repetitive activity upon intracellular pH, sodium and contraction in sheep cardiac Purkinje fibres. J. Physiol. *398*, 341–360.

Brandes, R., and Bers, D.M. (1996). Increased work in cardiac trabeculae causes decreased mitochondrial NADH fluorescence followed by slow recovery. Biophys. J. *71*, 1024–1035. https://doi.org/10.1016/S0006-3495(96)79303-7.

Brandes, R., and Bers, D.M. (1997). Intracellular Ca2+ increases the mitochondrial NADH concentration during elevated work in intact cardiac muscle. Circ. Res. *80*, 82–87. https://doi.org/10.1161/01.res.80.1.82.

Buckler, K.J., and Vaughan-Jones, R.D. (1990). Application of a new pH-sensitive fluoroprobe (carboxy-SNARF-1) for intracellular pH measurement in small, isolated cells. Pflugers Arch. *417*, 234–239.

Casey, J.R., Grinstein, S., and Orlowski, J. (2010). Sensors and regulators of intracellular pH. Nat. Rev. Mol. Cell Biol. *11*, 50–61. https://doi.org/10.1038/nrm2820.

Ch'en, F.F., Dilworth, E., Swietach, P., Goddard, R.S., and Vaughan-Jones, R.D. (2003). Temperature dependence of Na+-H+ exchange, Na+-HCO3- co-transport, intracellular buffering and intracellular pH in Guinea-pig ventricular myocytes. J. Physiol. *552*, 715–726. https://doi.org/10.1113/jphysiol.2003.051888.

Cordat, E., and Casey, J.R. (2009). Bicarbonate transport in cell physiology and disease. Biochem. J. *417*, 423–439. https://doi.org/10.1042/BJ20081634.

Crampin, E.J., Smith, N.P., Langham, A.E., Clayton, R.H., and Orchard, C.H. (2006). Acidosis in models of cardiac ventricular myocytes. Philos. Trans. A Math. Phys. Eng. Sci. *364*, 1171–1186. https://doi.org/10.1098/rsta.2006.1763.

Dedkova, E.N., and Blatter, L.A. (2013). Calcium signaling in cardiac mitochondria. J. Mol. Cell Cardiol. *58*, 125–133. https://doi.org/10.1016/j.yjmcc.2012.12.021.

Doenst, T., Nguyen, T.D., and Abel, E.D. (2013). Cardiac metabolism in heart failure: implications beyond ATP production. Circ. Res. *113*, 709–724. https://doi.org/10.1161/CIRCRESAHA.113.300376.

Elliott, A.C., Smith, G.L., and Allen, D.G. (1994). The metabolic consequences of an increase in the frequency of stimulation in isolated ferret hearts. J. Physiol. *474*, 147–159. https://doi.org/10.1113/jphysiol.1994.sp020009.

Ellis, D., and Thomas, R.C. (1976a). Direct measurement of the intracellular pH of mammalian cardiac muscle. J. Physiol. *262*, 755–771.

Ellis, D., and Thomas, R.C. (1976b). Microelectrode measurement of the intracellular pH of mammalian heart cells. Nature *262*, 224–225.

Garlick, P.B., Radda, G.K., and Seeley, P.J. (1979). Studies of acidosis in the ischaemic heart by phosphorus nuclear magnetic resonance. Biochem. J. *184*, 547–554.

Harrison, S.M., Frampton, J.E., McCall, E., Boyett, M.R., and Orchard, C.H. (1992). Contraction and intracellular Ca2+, Na+, and H+ during acidosis in rat ventricular myocytes. Am. J. Physiol. *262*, C348–C357.

Hegyi, B., Chen-Izu, Y., Jian, Z., Shimkunas, R., Izu, L.T., and Banyasz, T. (2015). KN-93 inhibits IKr in mammalian cardiomyocytes. J. Mol. Cell Cardiol. *89*, 173–176. https://doi.org/10.1016/j.yjmcc.2015.10.012.

Hulikova, A., and Swietach, P. (2016). Nuclear proton dynamics and interactions with calcium signaling. J. Mol. Cell Cardiol. *96*, 26–37. https://doi.org/10.1016/j.yjmcc.2015.07.003.

Hunjan, S., Mason, R.P., Mehta, V.D., Kulkarni, P.V., Aravind, S., Arora, V., and Antich, P.P. (1998). Simultaneous intracellular and extracellular pH measurement in the heart by 19F NMR of 6-fluoropyridoxol. Magn. Reson. Med. *39*, 551–556.

Jian, Z., Chen, Y.J., Shimkunas, R., Jian, Y., Jaradeh, M., Chavez, K., Chiamvimonvat, N., Tardiff, J.C., Izu, L.T., Ross, R.S., and Chen-Izu, Y. (2016). In vivo cannulation methods for cardiomyocytes isolation from heart disease models. PLoS One *11*, e0160605. https://doi.org/10.1371/journal.pone.0160605.

Jian, Z., Han, H., Zhang, T., Puglisi, J., Izu, L.T., Shaw, J.A., Onofiok, E., Erickson, J.R., Chen, Y.J., Horvath, B., et al. (2014). Mechanochemotransduction during cardiomyocyte contraction is mediated by localized nitric oxide signaling. Sci. Signal. *7*, ra27. https://doi.org/10.1126/scisignal.2005046.

Kanaya, N., Murray, P.A., and Damron, D.S. (2006). Effects of L-type Ca2+ channel modulation on direct myocardial effects of diazepam and midazolam in adult rat ventricular myocytes. J. Anesth. *20*, 17–25. https://doi.org/10.1007/s00540-005-0356-7.

Kim, H.J., Myers, R., Sihn, C.R., Rafizadeh, S., and Zhang, X.D. (2013). Slc26a6 functions as an electrogenic Cl/HCO3 exchanger in cardiac myocytes. Cardiovasc. Res. *100*, 383–391. https://doi.org/10.1093/Cvr/Cvt195.

Kirschenlohr, H.L., Metcalfe, J.C., Morris, P.G., Rodrigo, G.C., and Smith, G.A. (1988). Ca2+ transient, Mg2+, and pH measurements in the cardiac cycle by 19F NMR. Proc. Natl. Acad. Sci. U S A *85*, 9017–9021. https://doi.org/10.1073/pnas.85.23.9017.

Kovacs, M., Toth, J., Hetenyi, C., Malnasi-Csizmadia, A., and Sellers, J.R. (2004). Mechanism of blebbistatin inhibition of myosin II. J. Biol. Chem. *279*, 35557–35563. https://doi.org/10.1074/jbc.M405319200.

Kushmerick, M.J. (1997). Multiple equilibria of cations with metabolites in muscle bioenergetics. Am. J. Physiol. *272*, C1739–C1747. https://doi.org/10.1152/ajpcell.1997.272.5.C1739.

Lavallee, M. (1964). Intracellular pH of rat atrial muscle fibers measured by glass micropipette electrodes. Circ. Res. *15*, 185–193.

Leem, C.H., Lagadic-Gossmann, D., and Vaughan-Jones, R.D. (1999). Characterization of intracellular pH regulation in the Guinea-pig ventricular myocyte. J. Physiol. *517*, 159–180.

Lu, X., Ginsburg, K.S., Kettlewell, S., Bossuyt, J., Smith, G.L., and Bers, D.M. (2013). Measuring local gradients of intramitochondrial [Ca(2+)] in cardiac myocytes during sarcoplasmic reticulum Ca(2+) release. Circ. Res. *112*, 424–431. https://doi.org/10.1161/CIRCRESAHA.111.300501.

Malmqvist, U.P., Aronshtam, A., and Lowey, S. (2004). Cardiac myosin isoforms from different species have unique enzymatic and mechanical properties. Biochemistry *43*, 15058–15065. https://doi.org/10.1021/bi0495329.

Masereel, B., Pochet, L., and Laeckmann, D. (2003). An overview of inhibitors of Na(+)/H(+) exchanger. Eur. J. Med. Chem. *38*, 547–554. https://doi.org/10.1016/s0223-5234(03)00100-4.

Neary, M.T., Ng, K.E., Ludtmann, M.H., Hall, A.R., Piotrowska, I., Ong, S.B., Hausenloy, D.J., Mohun, T.J., Abramov, A.Y., and Breckenridge, R.A. (2014). Hypoxia signaling controls postnatal changes in cardiac mitochondrial morphology and function. J. Mol. Cell Cardiol. *74*, 340–352. https://doi.org/10.1016/j.yjmcc.2014.06.013.

Niederer, S.A., Swietach, P., Wilson, D.A., Smith, N.P., and Vaughan-Jones, R.D. (2008). Measuring and modeling chloride-hydroxyl exchange in the Guinea-pig ventricular myocyte. Biophys. J. *94*, 2385–2403, S0006-3495(08)70582-4 [pii]10.1529/biophysj.107.118885.

Orchard, C.H., and Kentish, J.C. (1990). Effects of changes of pH on the contractile function of cardiac muscle. Am. J. Physiol. *258*, C967–C981.

Robert, V., Gurlini, P., Tosello, V., Nagai, T., Miyawaki, A., Di Lisa, F., and Pozzan, T. (2001). Beat-to-beat oscillations of mitochondrial [Ca2+] in cardiac cells. EMBO J. *20*, 4998–5007. https://doi.org/10.1093/emboj/20.17.4998.

Roos, A., and Boron, W.F. (1981). Intracellular pH. Physiol. Rev. *61*, 296–434.

Santo-Domingo, J., and Demaurex, N. (2012). Perspectives on: SGP symposium on mitochondrial physiology and medicine: the renaissance of mitochondrial pH. J. Gen. Physiol. *139*, 415–423. https://doi.org/10.1085/jgp.201110767.

Schroeder, M.A., Swietach, P., Atherton, H.J., Gallagher, F.A., Lee, P., Radda, G.K., Clarke, K., and Tyler, D.J. (2010). Measuring intracellular pH in the heart using hyperpolarized carbon dioxide and bicarbonate: a 13C and 31P magnetic resonance spectroscopy study. Cardiovasc. Res. *86*, 82–91. https://doi.org/10.1093/cvr/cvp396.

Sirish, P., Ledford, H.A., Timofeyev, V., Thai, P.N., Ren, L., Kim, H.J., Park, S., Lee, J.H., Dai, G., Moshref, M., et al. (2017). Action potential shortening and impairment of cardiac function by ablation of Slc26a6. Circ. Arrhythm. Electrophysiol. *10*. https://doi.org/10.1161/CIRCEP.117.005267.

Steenbergen, C., Deleeuw, G., Rich, T., and Williamson, J.R. (1977). Effects of acidosis and ischemia on contractility and intracellular pH of rat heart. Circ. Res. *41*, 849–858.

Swietach, P., Leem, C.H., Spitzer, K.W., and Vaughan-Jones, R.D. (2005). Experimental generation and computational modeling of intracellular pH gradients in cardiac myocytes. Biophys. J. *88*, 3018–3037. https://doi.org/10.1529/biophysj.104.051391.

Swietach, P., and Vaughan-Jones, R.D. (2005a). Relationship between intracellular pH and proton mobility in rat and Guinea-pig ventricular myocytes. J. Physiol. *566*, 793–806. https://doi.org/10.1113/jphysiol.2005.086165.

Swietach, P., and Vaughan-Jones, R.D. (2005b). Spatial regulation of intracellular pH in the ventricular myocyte. Ann. N. Y Acad. Sci. *1047*, 271–282. https://doi.org/10.1196/annals.1341.024.

Thai, P.N., Daugherty, D.J., Frederich, B.J., Lu, X., Deng, W., Bers, D.M., Dedkova, E.N., and Schaefer, S. (2018). Cardiac-specific conditional knockout of the 18-kDa mitochondrial translocator protein protects from pressure overload induced heart failure. Scientific Rep. *8*, 16213. https://doi.org/10.1038/s41598-018-34451-2.

Thomas, R.C. (1984). Experimental displacement of intracellular pH and the mechanism of its subsequent recovery. J. Physiol. *354*, 3P–22P.

Thorsen, K., Dam, V.S., Kjaer-Sorensen, K., Pedersen, L.N., Skeberdis, V.A., Jurevicius, J., Treinys, R., Petersen, I., Nielsen, M.S., Oxvig, C., et al. (2017). Loss-of-activity-mutation in the cardiac chloride-bicarbonate exchanger AE3 causes short QT syndrome. Nat. Commun. *8*, 1696. https://doi.org/10.1038/s41467-017-01630-0.

Turina, P., Samoray, D., and Graber, P. (2003). H+/ATP ratio of proton transport-coupled ATP synthesis and hydrolysis catalysed by CF0F1-liposomes. EMBO J. *22*, 418–426. https://doi.org/10.1093/emboj/cdg073.

Valkovic, L., Clarke, W.T., Schmid, A.I., Raman, B., Ellis, J., Watkins, H., Robson, M.D., Neubauer, S., and Rodgers, C.T. (2019). Measuring inorganic phosphate and intracellular pH in the healthy and hypertrophic cardiomyopathy hearts by in vivo 7T (31)P-cardiovascular magnetic resonance spectroscopy. J. Cardiovasc. Magn. Reson. *21*, 19. https://doi.org/10.1186/s12968-019-0529-4.

Vaughan-Jones, R.D. (1979). Regulation of chloride in quiescent sheep-heart Purkinje fibres studied using intracellular chloride and pH-sensitive micro-electrodes. J. Physiol. *295*, 111–137.

Vaughan-Jones, R.D., Peercy, B.E., Keener, J.P., and Spitzer, K.W. (2002). Intrinsic H(+) ion mobility in the rabbit ventricular myocyte. J. Physiol. *541*, 139–158.

Vaughan-Jones, R.D., Spitzer, K.W., and Swietach, P. (2006). Spatial aspects of intracellular pH regulation in heart muscle. Prog. Biophys. Mol. Biol. *90*, 207–224. https://doi.org/10.1016/j.pbiomolbio.2005.06.004.

Vaughan-Jones, R.D., Spitzer, K.W., and Swietach, P. (2009). Intracellular pH regulation in heart. J. Mol. Cell Cardiol. *46*, 318–331. https://doi.org/10.1016/j.yjmcc.2008.10.024.

Waddell, W.J., and Bates, R.G. (1969). Intracellular pH. Physiol. Rev. *49*, 285–329. https://doi.org/10.1152/physrev.1969.49.2.285.

Walley, K.R., Lewis, T.H., and Wood, L.D. (1990). Acute respiratory acidosis decreases left ventricular contractility but increases cardiac output in dogs. Circ. Res. *67*, 628–635. https://doi.org/10.1161/01.res.67.3.628.

Wang, H.S., Chen, Y., Vairamani, K., and Shull, G.E. (2014). Critical role of bicarbonate and bicarbonate transporters in cardiac function.

World J. Biol. Chem. *5*, 334–345. https://doi.org/10.4331/wjbc.v5.i3.334.

Wang, Z., Ying, Z., Bosy-Westphal, A., Zhang, J., Schautz, B., Later, W., Heymsfield, S.B., and Muller, M.J. (2010). Specific metabolic rates of major organs and tissues across adulthood: evaluation by mechanistic model of resting energy expenditure. Am. J. Clin. Nutr. *92*, 1369–1377. https://doi.org/10.3945/ajcn.2010.29885.

Wiersma, M., van Marion, D.M.S., Wust, R.C.I., Houtkooper, R.H., Zhang, D., Groot, N.M.S., Henning, R.H., and Brundel, B. (2019). Mitochondrial dysfunction underlies cardiomyocyte remodeling in experimental and clinical atrial fibrillation. Cells *8*. https://doi.org/10.3390/cells8101202.

Zervou, S., Whittington, H.J., Russell, A.J., and Lygate, C.A. (2016). Augmentation of creatine in the heart. Mini Rev. Med. Chem. *16*, 19–28. https://doi.org/10.2174/1389557515666150722102151.

Zou, Y., Yao, A., Zhu, W., Kudoh, S., Hiroi, Y., Shimoyama, M., Uozumi, H., Kohmoto, O., Takahashi, T., Shibasaki, F., et al. (2001). Isoproterenol activates extracellular signal-regulated protein kinases in cardiomyocytes through calcineurin. Circulation *104*, 102–108. https://doi.org/10.1161/hc2601.090987.

STAR★METHODS

KEY RESOURCES TABLE

REAGENT or RESOURCE	SOURCE	IDENTIFIER
Chemicals, peptides, and recombinant proteins		
pHrodo™ Green AM	ThermoFisher Scientific	P35373
Carboxy SNARF®-1 AM	ThermoFisher Scientific	C1272
(±)-Blebbistatin	Abcam	Ab120425
2,3-Butanedione monoxime	Sigma-Aldrich, USA	B0753
(-)-Isoproterenol hydrochloride	Sigma-Aldrich	I6504
5-(N-Ethyl-N-isopropyl) amiloride	Sigma-Aldrich	A3085
Rotenone	Sigma-Aldrich	R8875
Antimycin A	Sigma-Aldrich	A8674
2-[2-[4-(trifluoromethoxy) phenyl] hydrazinylidene]-propanedinitrile (FCCP)	Sigma-Aldrich	C2920
Verapamil hydrochloride	Sigma-Aldrich	V4629
Collagenase type II	Worthington, USA	LS004176
Protease type XIV	Sigma-Aldrich	P5147
Ketamine hydrochloride injection (100mg/ml)	Akorn Inc., USA	NDC 50989-161-06
Xylazine sterile solution (20mg/ml)	Akorn Inc., USA	NDC59399-110-20
Heparin (1000 USP units/ml)	Fresenius Kabi USA, LLC	NDC63323-540-57
Fetal bovine serum	ThermoFisher Scientific	10437028
Penicillin-Streptomycin	ThermoFisher Scientific	15-140-122
Novolin R human insulin	Novo Nordisk USA	NDC 0169-1833-11
Bovine serum albumin	Sigma-Aldrich	A9418
Other salt and chemicals	Sigma-Aldrich	https://www.sigmaaldrich.com
Experimental models: organisms/strains		
New Zealand white rabbits	Western Oregon Rabbit Company	2495 Rosecrest Dr, Philomath, OR 97370, USA
C57BL/6J mice	The Jackson Laboratory	https://www.jax.org
Software and algorithms		
IonWizard (64-bit) 7.2.7.138	IonOptix	https://www.ionoptix.com
GraphPad Prism 9	GraphPad Software	https://www.graphpad.com
Origin Pro 2021	OriginLab Corp., Northampton, MA	https://www.originlab.com
BioRender	BioRender	https://www.biorender.com

RESOURCE AVAILABILITY

Lead contact

Further information and requests for resources and reagents should be directed to and will be fulfilled by the lead contact, Xiao-Dong Zhang (xdzhang@ucdavis.edu).

Materials availability

All unique reagents generated in this study are available from the Lead Contact with a completed Materials Transfer Agreement.

Data and code availability

The data supporting the current study have not been deposited in a public repository because they are only used for the publication of this manuscript. This paper does not report original code. Any additional

information required to reanalyze the data reported in this paper is available from the lead contact upon request.

EXPERIMENTAL MODEL AND SUBJECT DETAILS

All animal care and procedures were performed in accordance with the protocols approved by the Institutional Animal Care and Use Committee of the University of California, Davis, and per National Institutes of Health guidelines. Male and female animals were used. All experiments described in the study were conducted in a blinded fashion with different investigators for animal handlings, cardiomyocyte isolations, data collection and analysis. The cardiomyocytes used for each experiment were isolated from ~68 rabbits (New Zealand White rabbits, male, 3-6 months of old with 2-5 kg of body weight, Western Oregon Rabbit Company, Philomath, OR, USA) and ~21 mice (C57 BL/6J, male and female, 10-16 weeks old, Jackson Laboratory, Bar Harbor, ME, USA) depending on the sample size, and randomly assigned to the experimenters.

METHOD DETAILS

Cell isolation and chemicals

The chemicals were purchased from Sigma-Aldrich (St. Louis, MO, USA) unless specifically indicated. Blebbistatin was purchased from Abcam (Abcam, Cambridge, UK). Rabbit and mouse cardiomyocytes were isolated using the method we reported(Bartos et al., 2017; Hegyi et al., 2015; Jian et al., 2016; Kim et al., 2013; Sirish et al., 2017). Rabbit cardiomyocytes were isolated from hearts excised from New Zealand White rabbits. Briefly, rabbits were administered heparin at 400 USP units per kg subcutaneously 15–30 min before surgery. The animal was anesthetized with isoflurane inhalation (3-5%). The heart was excised and washed in a cold perfusion solution containing (in mM): 140 NaCl, 5.4 KCl, 1 $MgCl_2$, 5 Glucose, 5 HEPEs (free acid), 5 HEPEs (sodium salt), and pH 7.4, supplemented with 40 units of Novolin R human insulin, 50,000 units penicillin, and 50,000 micrograms of streptomycin per litter, and was then cannulated and mounted on a Langendorff apparatus. The heart was initially perfused with perfusion solution with added 2800 USP heparin per litter for 5 min to clear the blood. The heart was then perfused with perfusion solution with added collagenase type II (1 mg/ml Worthington Biochemical Corporation, Lakewood, NJ, USA), protease Type XIV (0.04 mg/ml, Sigma Aldrich, St. Louis, MO, USA), 5 mM taurine, and 0.02 mM $CaCl_2$ under constant flow (3-6 ml/min/gram heart weight) until it loses most of its integrity (typically 25-30 min). The temperature of the perfusion solutions was kept at 37°C. The heart was then removed from the perfusion system, and the digestion was stopped by incubation of the heart in perfusion solution with added 10% fetal bovine serum (FBS) and 0.02 mM $CaCl_2$. The ventricles and atria were minced and pipetted in the solution to liberate individual ventricular and atrial myocytes as needed. Cells were filtered through nylon mesh, and stored in perfusion solution with added 0.125 mM $CaCl_2$ at room temperature for experimental use. Isolation of mouse cardiomyocytes followed the conventional enzymatic dissociation methods we reported (Jian et al., 2016; Sirish et al., 2017). Mice were anesthetized by intraperitoneal injection of 80 mg/kg of ketamine and 5 mg/kg of xylazine. Intraperitoneal administration of 300 USP units of heparin was performed 10-15 minutes before the surgery. Mice were exsanguinated by rapid heart excision. The excised heart was quickly immersed in the perfusion solution containing (in mM): 113 NaCl, 4.7 KCl, 1.2 $MgSO_4$, 0.6 Na_2HPO_4, 0.6 KH_2PO4, 12 $NaHCO_3$, 10 $KHCO_3$, 30 Taurine, 10 Hepes, and 10 glucose, and pH = 7.4. After trimming off the associated tissues, the heart was cannulated on a Langendorff apparatus and first perfused with perfusion solution. After 3 min, the heart was perfused with perfusion solution with added collagenase (1 mg/mL, type II, Worthington Biochemical Corporation, Lakewood, NJ, USA). The perfusion pressure was monitored, and the flow rate was adjusted to maintain the initial perfusion pressure at ≈ 60 mmHg. The temperature of the perfusion solutions was kept at 37°C. After 15 to 20 min of collagenase digestion, the heart was then removed from the perfusion apparatus and transferred to petri dish containing perfusion solution with the addition of 10% FBS. The ventricles and atria were minced and pipetted to obtain ventricular and atrial myocytes, respectively. Cells were harvested by filtering through nylon mesh, and the Ca^{2+} concentration in the cell storage solution was restored stepwise using solutions containing 0.2, 0.5, or 1 mM Ca^{2+} (in mM): 133.5 NaCl, 4 KCl, 1.2 NaH_2PO_4, 10 HEPES, 1.2 $MgSO_4$, 10 glucose, 20 taurine, 0.2 (or 0.5, or 1) $CaCl_2$, pH = 7.4, supplemented with bovine serum albumin (1 mg/ml). Cardiomyocytes were maintained in the cell storage solution containing 1 mM Ca^{2+} at room temperature until ready for experiments.

Measurement of pH_i and sarcomere length

We used IonOptix contractility (IonOptix LLC., Westwood, MA, USA) system(Jian et al., 2014; Sirish et al., 2017) to measure single cardiomyocyte contraction and pH_i. Cardiomyocytes were loaded with SNARF-1

AM (ThermoFisher Scientific, Waltham, MA, USA) or pHrodo green (ThermoFisher Scientific, Waltham, MA, USA) before pH_i measurement. For pH_i measurement, cardiomyocytes were first incubated for 5 minutes in Ca^{2+}-free Tyrode's solution containing (in mM): 120 NaCl, 24 Na-Glutamate, 4 KCl, 1 $MgCl_2$, 10 Glucose, 0.33 NaH_2PO_4, 10 HEPES, and pH 7.4, with added either 5 μM SNARF-1 AM or 5 μM pHrodo greenfor dye loading. After removing the loading solution, cardiomyocytes were washed twice using Tyrode's solution and resuspended with Tyrode's solution for pH measurement. To reduce the effects of photobleaching and dye leakage of pHrodo green on the measurement with longer duration, we recorded on pHrodo green loaded cardiomyocytes without any interventions for ~10 mins with pacing and without pacing, and the photobleaching process of the fluorescencent signal was well fitted by a linear equation (Figure S1). The slope resulting from the linear fitting was used to correct the pH measurement to minimize the effects of photobleaching and dye leakage by subtracting the slope factor.

Cardiomyocytes were seeded in a chamber with two field stimulation electrodes connected to a Myopacer (IonOptix LLC., Westwood, MA, USA). The chamber was mounted on the stage of the Zeiss Axio Observer A1 inverted fluorescent microscope imaged by using a 63× or 40× oil lens. The chamber was perfused continuously during recordings. Cardiomyocytes were paced with a square bipolar pulse with 2 ms width and 10 V amplitude at different frequencies ranging from 0.1 Hz to 4 Hz. The measurement was performed at room temperature (RT, 20–22°C) and 36°C. The temperature control was achieved by using Warner TC-344C temperature controller (Warner Instruments, Holliston, MA, USA). The signals were acquired by IonWizard 7 software.

For the measurement of pH_i, a xenon lamp was used as an excitation light source. For SNARF-1 measurement, the dye loaded cardiomyocytes were excited by a selected wavelength of 550 ± 10 nm as previously reported(Buckler and Vaughan-Jones, 1990), and the emitted fluorescent light was split by a 605 nm long-pass dichroic mirror with the shorter wavelengths through a band-pass filter of 585 ± 10 nm, and the longer wavelengths through a band-pass filter of 630 ± 15 nm to two photomultipliers, respectively. For pHrodo green measurement, the dye loaded cardiomyocytes were excited by a selected wavelength of 500 ± 10 nm, and the emitted fluorescent light was filtered using a band-pass filter of 535 ± 15 nm and collected by a photomultiplier. The contraction was measured using a high-speed camera (MyoCam-S, 240 to 1000 frames/s) to record the sarcomere movement. The sarcomere pattern was used to calculate the sarcomere length using an FFT algorithm.

The solutions for pH measurement include Tyrode's solution buffered by HEPES containing (in mM): 120 NaCl, 24 Na-Glutamate, 4 KCl, 1 $MgCl_2$, 2 $CaCl_2$, 10 Glucose, 0.33 NaH_2PO_4, 10 HEPES, and pH 7.4, and Tyrode's solution buffered by HCO_3^- containing (in mM): 120 NaCl, 4 KCl, 2 $CaCl_2$, 0.33 NaH_2PO_4, 1 $MgCl_2$, 10 Glucose, 24 $NaHCO_3$, gassed by 5% CO_2 and 95% O_2. To reduce the Cl^- concentration, NaCl was replaced by an equal concentration of Na-Glutamate. To test the effects of ammonium and acetate, 10 mM NH_4Cl or 20 mM sodium acetate was added to the $NaHCO_3$-buffered Tyrode's solution, and the osmolarity of the control solution was balanced by adding equal molar of D-mannitol. For the solution with 20 mM sodium acetate, 10 μM 5-(N-Ethyl-N-isopropyl) amiloride (EIPA, a specific inhibitor of sodium-proton exchanger, NHE) was added before use to inhibit the NHE activation during recording. If not indicated, the recordings were all performed in HCO_3^--buffered Tyrode's solution. The calibration solutions contained (in mM): 140 KCl, 1 $MgCl_2$, 20 HEPES (or MES at pH 5.5), with pH 5.5, 6.5, 7.5, 8.5. Nigericin, a K^+/H^+ antiporter ionophore, (10 μM) was added to the calibration solution before use.

The SNARF-1 emission ratio (F_{580}/F_{640}) was converted to a pH_i value using standard calibration(Blank et al., 1992; Buckler and Vaughan-Jones, 1990; Niederer et al., 2008; Sirish et al., 2017). The pHrodo green intensity was converted to a pH_i value using the calibration method provided by the manufacturer. The calibration was performed by measuring the SNARF-1 emission ratios and pHrodo green intensities when the cells were perfused by calibration solutions with four different pH values of 5.5, 6.5, 7.5, and 8.5 (Figure S2). For pHrodo green calibration, the fluorescence intensity signals were normalized by the peak intensity at pH 5.5, and pH recordings performed on each cardiomyocyte were completed by perfusion using pH 5.5 calibration solution to acquire the peak fluorescence intensity value for normalization and proper calibration for each cardiomyocyte. The normalized intensities at calibration solutions were fitted by a sigmoidal function to obtain the standard calibration curve for pHrodo green (Figure S2B). The representative pHrodo green and SNARF-1 fluorescence signals recorded in rabbit cardiomyocytes are shown in Figures S2A and S2C. The representative calibration trace and calibration curve for SNARF-1 are shown in Figure S2D.

Ten cycles of the pH_i transients and sarcomere shortening traces were averaged and used for analyses. The representative traces shown in the figures were chosen to represent the mean values of the experimental group if applicable.

To ensure that the changes in fluorescence signals were not due to motion artifacts introduced by cell contractions, we positioned the relaxed cell completely within the imaging frame using either 63× or 40× objectives depending on the cell size. After each measurement, the cardiomyocyte was moved away from the imaging frame for recording background fluorescence signals, and background fluorescence signals were subtracted for each channel during the data analysis. For pacing experiment, we did not count the cardiomyocytes that have less than 50% of averaged normal fractional shortening at lowest pacing rate.

To quantify the cytosolic dye loading, the loaded cells were perfused by Tyrode's solution containing 50 μg/ml saponin. Only (10.5 ± 1.4)% (pHrodo green, n = 7), (7.5 ± 1.5)% (SNARF-1/F580, n = 8), (8.1 ± 1.6)% (SNARF-1/F640, n = 8) fluorescence signals remained after saponin treatment, suggesting predominant cytosolic dye loading. The intrinsic fluorescence signals of cardiomyocytes were measured before the loading of the dye, and the ratios of the intrinsic signals to the dye signals were quantified and are less than one percent (pHrodo green: (0.78 ± 0.35)%; SNARF-1 F580: (0.92 ± 0.27)%, F640: (0.62 ± 0.27)%). The intrinsic fluorescence signal is subtracted from the dye signals.

QUANTIFICATION AND STATISTICAL ANALYSIS

We estimate a sample size of 5 per experiment to detect at least 15% difference before and after the change of the conditions with alpha=0.05 for a two-tailed test to give the power of the study >0.95, assuming the standard deviation of the differences to be 5% (SigmaStat, Systat Software Inc.). No data were excluded. Data are presented as mean ± S.E.M. Shapiro-Wilk test was used for normality test. Statistical comparisons were achieved by one-way ANOVA combined with Tukey's post hoc analyses among three or more groups, or paired sample *t*-test (two-tailed) or two-sample *t*-test when the data follow a normal distribution, if comparing the effects before and after the application of drugs on the same cell. If the data did not follow a normal distribution or with small sample number, non-parametric paired Wilcoxon signed-rank test was used. Statistical significance was set at $p < 0.05$. The statistical analyses were performed using Origin Pro 2021 (OriginLab, Northampton MA, USA) and GraphPad Prism 9 (GraphPad Software, San Diego, CA, USA).